An RNA exosome subunit mediates cell-to-cell trafficking of a homeobox mRNA via plasmodesmata

Munenori Kitagawa[1], Peipei Wu[1], Rachappa Balkunde[1]†, Patrick Cunniff[1] and David Jackson[1,2]*.

[1]Cold Spring Harbor Laboratory, Cold Spring Harbor, NY 11724, USA.

[2]National Key Laboratory of Crop Genetic Improvement, Huazhong Agricultural University, Wuhan 430070, PR China.

† Present address: Bayer Crop Science LLC, Chesterfield, MO 63017, USA.

*Correspondence to: jacksond@cshl.edu. http://orcid.org/0000-0002-4269-7649

Abstract

mRNAs function as mobile signals for cell-to-cell communication in multicellular organisms. The KNOTTED1 (KN1) homeodomain family transcription factors act non-cell-autonomously to control stem cell maintenance in plants, via cell-to-cell movement of their proteins and mRNAs through plasmodesmata, however the mechanism of mRNA movement is largely unknown. Here we show that cell-to-cell movement of a KN1 mRNA requires Ribosomal RNA-Processing Protein 44A (AtRRP44A), a subunit of the RNA exosome that processes or degrades diverse RNAs in eukaryotes. AtRRP44A can interact with plasmodesmata and mediates the cell-to-cell trafficking of KN1 mRNA, and genetic analysis indicates that AtRRP44A is required for the developmental functions of SHOOT MERISTEMLESS, an Arabidopsis KN1 homolog. Our findings suggest that AtRRP44A promotes mRNA trafficking through plasmodesmata to control stem cell-dependent processes in plants.

One Sentence Summary:

RRP44 regulates cell-to-cell transport of a stem cell regulatory mRNA in plants.

Main text

Cell-to-cell communication in multicellular organisms promotes cell fate specification and coordination of development. As one way to transmit information between cells, plants selectively traffic transcription factors through plasmodesmata, cell wall embedded channels that connect the cytoplasm of neighboring cells (*1-3*). The maize KNOTTED1 (KN1) homeodomain transcription factor was the first mobile protein found to use this trafficking pathway (*4*). Previous studies have identified regulators of KN1 protein trafficking (*5-7*), however KN1 protein traffics with its mRNA (*4*). Selective trafficking of mRNAs in plants is prevalent (*8-12*), however the mechanism by which this occurs through plasmodesmata has not been addressed. Here, we identify Arabidopsis Ribosomal RNA-Processing Protein 44A (AtRRP44A) as an essential factor for the cell-to-cell trafficking of KN1 mRNA, and show that AtRRP44A-dependent mRNA trafficking is required for cell-to-cell protein trafficking and stem cell functions in plants.

Isolation of KN1 trafficking mutants

We previously established a genetic screen in Arabidopsis to identify regulators of KN1 cell-to-cell trafficking, using a "trichome rescue system" (*7, 13*). Trichomes are hairlike extensions of the leaf epidermis. Their development requires the cell-autonomous activity of GLABROUS1 (GL1), a MYB transcription factor (*14*). In our system, a fusion protein of green fluorescent protein (GFP), GL1, and the KN1 C-terminal trafficking domain ($KN1^{c}$) is expressed in the mesophyll cell layers of leaves of trichomeless *gl1* mutants using the *Rubisco small subunit 2b* promoter (*pRbcS::GFP~GL1~KN1*^{c}) (*7*). Trafficking of GFP~GL1~$KN1^{c}$ to the epidermis rescues trichome formation in this line, thus

trichome number is an output for KN1 trafficking. In an ethyl methanesulfonate (EMS) mutagenesis screen of trichome rescue lines, we isolated two mutants lacking trichomes, initially referred to as *rb31-7* and *mk5-140* (Fig. 1, A to C). Consistent with the loss of trichomes, epidermal GFP~GL1~KN1^{c} accumulation decreased significantly in the mutants (Fig. 1, D to F) despite similar expression compared to the parental control trichome rescue lines in mesophyll cell layers (Fig. 1, G to I). These observations suggest that both mutants reduced the trafficking of GFP ~GL1~KN1^{c} from the mesophyll cell layers to the epidermis. To ask if trichome loss in the mutants was simply due to a reduction in transgene expression, we measured GFP~GL1~KN1^{c} fluorescence in mesophyll cells of the mutants. We found that it was ~ 50-70% of the level in the parental trichome rescue lines (fig. S1A). However, this reduction was not the cause of trichome loss, because plants hemizygous for the trichome rescue transgene also had ~ 50% expression, and this was sufficient for trichome rescue (fig. S1, A and B). Thus, we confirmed that KN1 trafficking was inhibited in *rb31-7* and *mk5-140* mutants.

KN1 trafficking mutants encode AtRRP44A

Both *rb31-7* and *mk5-140* mutants behaved as single recessive loci. We mapped them by sequencing M3 pools of mutants or non-mutant siblings to ~44x coverage. Using the MutMap+ pipeline (*15*) we identified potentially causal point mutations of *rb31-7* and *mk5-140* within the same gene, At2g17510 (G to A and C to T, causing disruptive Cys551 to Tyr and Pro781 to Leu amino acid substitutions, respectively) (Fig. 1, J and K). At2g17510 encodes AtRRP44A, a subunit of the RNA exosome. We confirmed this as the causal gene by complementing trichome rescue defects in both mutants using a TagRFP-T (hereafter RFP) fusion protein expressed by its native regulatory sequences (*pAtRRP44A::AtRRP44A~RFP*) (Fig. 1, L and M), so we renamed our alleles as *atrrp44a-4* and *atrrp44a-5*, respectively. Null alleles of *AtRRP44A* in Arabidopsis are lethal (*16, 17*), as in yeast, Drosophila, and in human cells (*18-21*), thus ours are likely to be weak alleles. The RNA exosome is a

multiprotein complex involved in the processing and degradation of a wide range of RNAs in eukaryotes, and RRP44 is a catalytic subunit with 3'-to-5' exoribonuclease and endoribonuclease activities (*22-24*). Two conserved domains, RNB and PIN, are responsible for these activities, respectively (Fig. 1K). The mutations in *atrrp44a-4* and *atrrp44a-5* were in highly conserved residues in the RNB domain (Fig. 1K and fig. S2A) (*25-27*) in the vicinity of the RRP44 catalytic center (fig. S2B) (*28*), supporting an idea that they are important for function.

atrrp44a mutants enhance _stm_ and _cct8_ phenotypes

KN1 can fully complement the shoot meristem defects of its Arabidopsis homolog SHOOT MERISTEMLESS (STM), whose mobility is essential for meristem maintenance (*13, 29, 30*). *atrrp44a-5* mutants also blocked trichome rescue by a *GFP~GL1~STM*^{c} fusion, suggesting that AtRRP44A also participates in STM trafficking (fig. S3). Thus, we next asked if AtRRP44A affects STM function. *atrrp44a* mutants had no obvious defects in shoot meristem size (Fig. 2, A, B, and E, and fig. S4A), however they significantly enhanced the meristem phenotypes of *stm-10*, a weak allele of *stm (31)*. Shoot meristems of *atrrp44a-4*; *stm-10* double mutants were significantly smaller than *stm-10* single mutants (Fig. 2, A-E), and terminated in many of the *atrrp44a-5; stm-10* double mutant seedlings (22/24, fig. S4B). Similarly, meristems arrested in many of the *atrrp44a-4; stm-10* double mutants (fig. S4C), resulting in seedlings with fewer leaves (fig. S4D). Consistent with these phenotypes, expression of *STM* and of additional shoot meristem genes *CLAVATA3* (*CLV3*) and *WUSCHEL* appeared disorganized and/or reduced in the *atrrp44a; stm-10* double mutant meristems, and CLV3 expression was significantly lower in quantitative reverse transcription polymerase chain reaction (RT-qPCR) experiments (fig. S4, E and F). Collectively, our data suggest that AtRRP44A is required for STM dependent shoot meristem maintenance, perhaps by controlling STM RNA trafficking. To further support a role for *atrrp44a* in meristem development, we attempted to enhance

our weak alleles by combining in a hemizygous state with the *atrrp44a-1* null allele (Fig. 1J) (*17*). Indeed, these combinations significantly reduced the shoot meristem size (fig. S4G). We also assayed genetic interactions between *AtRRP44A* and *CCT8*, a regulator of KN1 trafficking (*7*) that is required for STM function in stem cell maintenance. The *atrrp44a; cct8-1* double mutants developed dwarf shoots with fasciated stems (Fig. 2, F and G, and fig. S5, N = 20/20 plants [*atrrp44a-4; cct8-1*]; 18/18 plants [*atrrp44a-5; cct8-1*]). The double mutants also occasionally made non-fasciated shoot branches, which terminated prematurely (Fig. 2H and fig. S5B, N = 10/20 plants [*atrrp44a-4; cct8-1*]; 11/18 plants [*atrrp44a-5; cct8-1*]). These phenotypes were not observed in the single mutants, suggesting that AtRRP44A regulates the balance of proliferation and differentiation in the shoot meristem through a chaperonin dependent pathway. Collectively, our data support the idea that AtRRP44A is required for the function and trafficking of KN1 and STM, which are essential for meristem maintenance.

AtRRP44A can localize to plasmodesmata

Given our hypothesis that AtRRP44A promotes cell-to-cell trafficking of STM, we next asked if its expression overlaps with STM in the shoot meristem. We transformed the native AtRRP44A~RFP fusion construct into plants heterozygous for the *atrrp44a-1* null allele. This fusion construct was functional, as it complemented lethality of the null allele in the subsequent generation (fig. S6A). AtRRP44A~RFP expression was observed throughout the shoot meristem and flower primordia (Fig. 3A and fig. S6B), overlapping with STM expression (*32*), as well as in epidermal and mesophyll layers of leaf primordia (Fig. 3B), where GFP~GL1~KN1^{c} traffics in the trichome rescue system. Thus, AtRRP44A was expressed broadly, including in the shoot meristem where STM traffics. The fusion protein accumulated in nuclei, as expected; mainly in the nucleolus in meristem cells and throughout the nucleoplasm in leaf primordia (Fig. 3, A and B) (*16*).

We next asked how AtRRP44A might facilitate trafficking. Previous studies using microinjection or the trichome rescue system indicated that KN1 protein promotes the trafficking of its mRNA (*4, 13*), suggesting KN1 protein and mRNA traffic as an mRNA-protein (mRNP) complex. AtRRP44A binds to the exosome core complex, which is involved in the processing of rRNAs, mRNAs and ncRNAs in Arabidopsis (*17, 33, 34*), but it is unclear whether AtRRP44A participates in mRNA degradation or processing (*17*). Nonetheless, since AtRRP44A is a ribonuclease, we asked if it might affect trafficking indirectly, by degradation or processing of KN1 or STM mRNA. However, when we examined mRNA levels and decay rates in dissected shoot apices or in seedlings by RT-qPCR, there were no differences in levels or stability of STM mRNA in *atrrp44a* mutants (fig. S7A-D). We also asked if the trafficking function of AtRRP44A could be uncoupled from its RNA processing activity, by introducing a non-catalytic AtRRP44A mutant (AtRRP44A^{D489N}~RFP) (*27*) driven by its native promoter into *atrrp44a* mutant trichome rescue plants. This construct fully rescued KN1 trafficking and trichome formation (fig. S7E-G). These results suggest that AtRRP44A function in trafficking or trichome rescue is unrelated to its potential role in mRNA processing or degradation, although whether this non-canonical function promotes RNA trafficking in the meristem remains to be tested. We next hypothesized that AtRRP44A might directly participate in KN1 or STM mRNA trafficking, for example, by recruiting their mRNA to plasmodesmata, or by transporting mRNA through plasmodesmata. Supporting these ideas, AtRRP44A is found in the Arabidopsis cell wall proteome (*35*) and the plasmodesmal proteome (*36*) despite its predominant accumulation in nuclei (Fig. 3, A, B, and D) (*16*), suggesting that a fraction of the protein may associate with plasmodesmata. We could not detect plasmodesmata localization using our native AtRRP44A tagged lines, so to test this possibility we modified the AtRRP44A~RFP fusion by deleting two nuclear localization signals (NLSs), and adding a nuclear export signal (NES) (AtRRP44A^{NLSΔ}~NES~RFP) to promote its export from the nucleus. Indeed, this modified protein accumulated outside of the nuclei (Fig. 3C and D). We

observed its localization in puncta that co-localized with aniline blue stained plasmodesmata (75% of plasmodesmata showed AtRRP44A^{NLSA}~NES~RFP signal, N = 227/302 plasmodesmata from 10 cells, Fig. 3, E and F, and fig. S6C). Thus, our data supports the idea that AtRRP44A interacts with plasmodesmata to promote trafficking.

AtRRP44A mediates KN1 mRNA trafficking

We next asked if AtRRP44A promotes mRNA trafficking, by visualizing KN1 mRNA in the trichome rescue system (*37*). We inserted 24 repeats of the MS2 bacteriophage binding sequence (MBS) between the KN1 stop codon and 3' UTR in our mesophyll expressed trichome rescue construct, to make *pRbcS::GFP~GL1~KN1^{c}~MBS*. This construct was introduced into plants that expressed an MS2 coat protein (MCP)~RFP fusion in the epidermis (Fig. 4A, epiMCP). MCP binds to MBS sequences, so if GFP~GL1~KN1^{c}~MBS mRNA traffics from the mesophyll to the epidermis, we expect to detect it through its binding by epiMCP~RFP in epidermal cells. Indeed, lines wild type (WT) for *AtRRP44A* showed many MCP~RFP puncta in the cytoplasm of epidermal cells (Fig. 4B) whereas plants that expressed MCP~RFP alone did not have puncta (fig. S8, A and B), indicating that GFP~GL1~KN1^{c}~MBS mRNA trafficked from mesophyll cell layers to the epidermis and formed fluorescent cytoplasmic puncta in association with MCP~RFP. In contrast, when we introduced the MBS/MCP system into *atrrp44a* mutants, their epidermal cells had ~ 8 fold fewer fluorescent puncta (Fig. 4C and D) despite similar levels of GFP~GL1~KN1^{c} protein in mesophyll cells (fig. S8, C and D). The puncta in *atrrp44a-5* were also smaller, suggesting they contained fewer GFP~GL1~KN1^{c}~MBS mRNA molecules (fig. S8E). To confirm this apparent loss of mRNA trafficking was not due to a reduction of GFP~GL1~KN1^{c}~MBS mRNA in *atrrp44a* mutants, we expressed MCP~RFP in mesophyll cell layers (mesoMCP, Fig. 4E). As expected, the mutants had similar numbers of KN1 mRNA puncta in mesophyll cells as the WT lines (Fig. 4, F-H). Thus, our data

suggest that AtRRP44A is required for the cell-to-cell trafficking of KN1 mRNA in the trichome system, although its contribution to RNA trafficking in the meristem remains to be tested. To support this role, we asked if AtRRP44A could bind to STM mRNA *in vivo*, using RNA immunoprecipitation (RIP)-qPCR from extracts of shoot apices of *pAtRRP44A::AtRRP44A~RFP; atrrp44a-1* plants. Indeed, we found that AtRRP44A was associated with STM transcripts *in vivo* (fig. S8F).

KN1 mRNA trafficking promotes protein trafficking

We next asked if KN1 mRNA trafficking was important in the selective transport of a KN1 signal, by scoring trichome rescue in the AtRRP44A wild type lines expressing mesoMCP~RFP (Fig. 4E). We reasoned that binding of MCP~RFP to GFP~GL1~KN1^{c}~MBS mRNA in mesophyll cells might inhibit its trafficking due to the large size of the mRNP complex, similar to a previous study (*38*). Indeed, trichome rescue was reduced in mesoMCP lines compared to epiMCP lines or our original trichome rescue lines without the MBS/MCP system (no MCP) (Fig. 4I). Consistently, GFP~GL1~KN1^{c} accumulation in the epidermis was also decreased in mesoMCP lines compared to epiMCP lines (Fig. 4, J and K; N = 16 plants from two independent transgenic lines). This result suggests that the cell-to-cell trafficking of KN1 mRNA promotes protein trafficking, for example as an mRNP complex, and/or the transported mRNA is translated *de novo* in the epidermis. Other homeodomain proteins also have the capacity to bind their mRNAs (*39*). Therefore, our data support the idea that AtRRP44A-mediated transport of a homeodomain mRNA plays a role in the cell-to-cell trafficking of a KN1 signal, possibly as an mRNP complex.

KN1 mRNA transiently associates with plasmodesmata

Finally, to support the idea that KN1 mRNA traffics cell-to-cell, we asked if KN1 mRNA associates with plasmodesmata, like other mobile mRNAs in plants (*40, 41*). By imaging the interface

between epidermal cells, we found co-localization of GFP~GL1~KN1^{c}~MBS mRNA with aniline blue stained plasmodesmata (Fig. 4L). Using time-lapse imaging, we found that KN1 mRNA puncta moved freely through the cytoplasm until they "met" a plasmodesma, where they paused for ~1-6 minutes before leaving (movies S1 and S2). We also observed KN1 mRNA-plasmodesmata interactions at the interface of epidermal and mesophyll cells (movie S3), and between leaf epidermal cells when expressed in a heterologous tobacco system (movie S4). Thus, our data support the idea that KN1 mRNA associates with plasmodesmata to traffic from cell to cell.

In summary, we demonstrate a role of KN1 mRNA trafficking in the selective transport of a KN1 signal, and the role of AtRRP44A in this process (fig. S9). This role of AtRRP44A appears to be independent of its function in RNA metabolism, and may involve additional factors that prevent its RNA processing activity, despite its binding to the mobile homeodomain mRNA. Our finding that trafficking of maize KN1 mRNA is mediated by AtRRP44A in Arabidopsis suggests that this mechanism is required for plant stem cell function in diverse plants. It remains to be seen whether RRP44A functions in transport of other plant mobile RNAs.

References and Notes

1. Z. P. Li, A. Paterlini, M. Glavier, E. M. Bayer, Intercellular trafficking via plasmodesmata: molecular layers of complexity. *Cellular and Molecular Life Sciences*, 1-18 (2020).
2. M. Kitagawa, D. Jackson, Plasmodesmata-mediated cell-to-cell communication in the shoot apical meristem: how stem cells talk. *Plants* **6**, 12 (2017).
3. J. O. Brunkard, P. C. Zambryski, Plasmodesmata enable multicellularity: new insights into their evolution, biogenesis, and functions in development and immunity. *Current Opinion in Plant Biology* **35**, 76-83 (2017).

4. W. J. Lucas *et al*., Selective trafficking of KNOTTED1 homeodomain protein and its mRNA through plasmodesmata. *Science* **270**, 1980-1983 (1995).
5. L. Liu *et al*., FTIP-dependent STM trafficking regulates shoot meristem development in Arabidopsis. *Cell reports* **23**, 1879-1890 (2018).
6. N. Winter, G. Kollwig, S. Zhang, F. Kragler, MPB2C, a microtubule-associated protein, regulates non-cell-autonomy of the homeodomain protein KNOTTED1. *The Plant Cell* **19**, 3001-3018 (2007).
7. X. M. Xu *et al*., Chaperonins facilitate KNOTTED1 cell-to-cell trafficking and stem cell function. *Science* **333**, 1141-1144 (2011).
8. L. Yang *et al*., m5C methylation guides systemic transport of messenger RNA over graft junctions in plants. *Current Biology* **29**, 2465-2476 (2019).
9. T. H. Ghate, P. Sharma, K. R. Kondhare, D. J. Hannapel, A. K. Banerjee, The mobile RNAs, StBEL11 and StBEL29, suppress growth of tubers in potato. *Plant molecular biology* **93**, 563-578 (2017).
10. K. J. Lu, N. C. Huang, Y. S. Liu, C. A. Lu, T. S. Yu, Long-distance movement of Arabidopsis *FLOWERING LOCUS T* RNA participates in systemic floral regulation. *RNA biology* **9**, 653-662 (2012).
11. M. Notaguchi, S. Wolf, W. J. Lucas, Phloem-mobile *Aux/IAA* transcripts target to the root tip and modify root architecture. *Journal of integrative plant biology* **54**, 760-772 (2012).
12. G. Kim, M. L. LeBlanc, E. K. Wafula, C. W. DePamphilis, J. H. Westwood, Genomic-scale exchange of mRNA between a parasitic plant and its hosts. *Science* **345**, 808-811 (2014).
13. J. Y. Kim, Y. Rim, J. Wang, D. Jackson, A novel cell-to-cell trafficking assay indicates that the KNOX homeodomain is necessary and sufficient for intercellular protein and mRNA trafficking. *Genes & Development* **19**, 788-793 (2005).

14. D. G. Oppenheimer, P. L. Herman, S. Sivakumaran, J. Esch, M. D. Marks, A *myb* gene required for leaf trichome differentiation in Arabidopsis is expressed in stipules. *Cell* **67**, 483-493 (1991).

15. R. Fekih *et al*., MutMap+: genetic mapping and mutant identification without crossing in rice. *PloS one* **8**, e68529 (2013).

16. W. Zhang, C. Murphy, L. E. Sieburth, Conserved RNaseII domain protein functions in cytoplasmic mRNA decay and suppresses Arabidopsis decapping mutant phenotypes. *Proceedings of the National Academy of Sciences* **107**, 15981-15985 (2010).

17. N. Kumakura, H. Otsuki, M. Tsuzuki, A. Takeda, Y. Watanabe, Arabidopsis AtRRP44A is the functional homolog of Rrp44/Dis3, an exosome component, is essential for viability and is required for RNA processing and degradation. *PLoS One* **8**, e79219 (2013).

18. H. Ohkura *et al*., Cold-sensitive and caffeine-supersensitive mutants of the *Schizosaccharomyces pombe dis* genes implicated in sister chromatid separation during mitosis. *The EMBO journal* **7**, 1465-1473 (1988).

19. M. J. Snee *et al*., Collaborative control of cell cycle progression by the RNA exonuclease Dis3 and Ras is conserved across species. *Genetics* **203**, 749-762 (2016).

20. R. Tomecki *et al*., Multiple myeloma-associated hDIS3 mutations cause perturbations in cellular RNA metabolism and suggest hDIS3 PIN domain as a potential drug target. *Nucleic acids research* **42**, 1270-1290 (2013).

21. P. Mitchell, E. Petfalski, A. Shevchenko, M. Mann, D. Tollervey, The exosome: a conserved eukaryotic RNA processing complex containing multiple 3′-> 5′ exoribonucleases. *Cell* **91**, 457-466 (1997).

22. C. Kilchert, "RNA exosomes and their cofactors" in *The Eukaryotic RNA Exosome*. (Springer, New York, 2020), pp. 215-235.

23. J. C. Zinder, C. D. Lima, Targeting RNA for processing or destruction by the eukaryotic RNA exosome and its cofactors. *Genes & development* **31**, 88-100 (2017).
24. C. Kilchert, S. Wittmann, L. Vasiljeva, The regulation and functions of the nuclear RNA exosome complex. *Nature Reviews Molecular Cell Biology* **17**, 227 (2016).
25. A. Dziembowski, E. Lorentzen, E. Conti, B. Séraphin, A single subunit, Dis3, is essentially responsible for yeast exosome core activity. *Nature structural & molecular biology* **14**, 15-22 (2007).
26. E. Lorentzen, J. Basquin, R. Tomecki, A. Dziembowski, E. Conti, Structure of the active subunit of the yeast exosome core, Rrp44: diverse modes of substrate recruitment in the RNase II nuclease family. *Molecular cell* **29**, 717-728 (2008).
27. N. Kumakura *et al*., Arabidopsis AtRRP44 has ribonuclease activity that is required to complement the growth defect of yeast *rrp44* mutant. *Plant Biotechnology* **33**, 77-85 (2016).
28. D. L. Makino, M. Baumgärtner, E. Conti, Crystal structure of an RNA-bound 11-subunit eukaryotic exosome complex. *Nature* **495**, 70-75 (2013).
29. J. Y. Kim, Z. Yuan, D. Jackson, Developmental regulation and significance of KNOX protein trafficking in Arabidopsis. *Development* **130**, 4351-4362 (2003).
30. R. Balkunde, M. Kitagawa, X. M. Xu, J. Wang, D. Jackson, SHOOT MERISTEMLESS trafficking controls axillary meristem formation, meristem size and organ boundaries in Arabidopsis. *The Plant Journal* **90**, 435-446 (2017).
31. S. Kanrar, O. Onguka, H. M. Smith, Arabidopsis inflorescence architecture requires the activities of KNOX-BELL homeodomain heterodimers. *Planta* **224**, 1163-1173 (2006).
32. J. A. Long, E. I. Moan, J. I. Medford, M. K. Barton, A member of the KNOTTED class of homeodomain proteins encoded by the *STM* gene of Arabidopsis. *Nature* **379**, 66-69 (1996).

33. H. Lange *et al*., The RNA helicases AtMTR4 and HEN2 target specific subsets of nuclear transcripts for degradation by the nuclear exosome in Arabidopsis thaliana. *PLoS Genet* **10**, e1004564 (2014).
34. J. A. Chekanova *et al*., Genome-wide high-resolution mapping of exosome substrates reveals hidden features in the Arabidopsis transcriptome. *Cell* **131**, 1340-1353 (2007).
35. E. M. Bayer *et al*., Arabidopsis cell wall proteome defined using multidimensional protein identification technology. *Proteomics* **6**, 301-311 (2006).
36. L. Fernandez-Calvino *et al*., Arabidopsis plasmodesmal proteome. *PloS one* **6**, e18880 (2011).
37. T. Lionnet *et al*., A transgenic mouse for *in vivo* detection of endogenous labeled mRNA. *Nature methods* **8**, 165-170 (2011).
38. G. Haimovich *et al*., Intercellular mRNA trafficking via membrane nanotube-like extensions in mammalian cells. *Proceedings of the National Academy of Sciences* **114**, E9873-E9882 (2017).
39. J. Dubnau, G. Struhl, RNA recognition and translational regulation by a homeodomain protein. *Nature* **379**, 694-699 (1996).
40. A. Sambade *et al*., Transport of TMV movement protein particles associated with the targeting of RNA to plasmodesmata. *Traffic* **9**, 2073-2088 (2008).
41. K. R. Luo, N. C. Huang, T. S. Yu, Selective targeting of mobile mRNAs to plasmodesmata for cell-to-cell movement. *Plant Physiology* **177**, 604-614 (2018).
42. S. J. Clough, A. F. Bent, Floral dip: a simplified method for Agrobacterium-mediated transformation of Arabidopsis thaliana. *The plant journal* **16**, 735-743 (1998).
43. A. M. Davis, A. Hall, A. J. Millar, C. Darrah, S. J. Davis, Protocol: Streamlined sub-protocols for floral-dip transformation and selection of transformants in Arabidopsis thaliana. *Plant Methods* **5**, 3 (2009).

44. F. Xu, C. Copeland, X. Li, Protein immunoprecipitation using *Nicotiana benthamiana* transient expression system. *Bio Protoc* **5**, e1520 (2015).

45. J. Chen, S. Dellaporta, "Urea-based plant DNA miniprep"in *The maize handbook*. (Springer, New York, 1994), pp. 526-527.

46. R. Zavaliev, B. L. Epel, "Imaging callose at plasmodesmata using aniline blue: quantitative confocal microscopy"in *Plasmodesmata*. (Springer, New York, 2015), pp. 105-119.

47. D. Jackson, B. Veit, S. Hake, Expression of maize *KNOTTED1* related homeobox genes in the shoot apical meristem predicts patterns of morphogenesis in the vegetative shoot. *Development* **120**, 405-413 (1994).

48. G. Wu, E. P. Spalding, Separate functions for nuclear and cytoplasmic cryptochrome 1 during photomorphogenesis of Arabidopsis seedlings. *Proceedings of the National Academy of Sciences* **104**, 18813-18818 (2007).

Acknowledgements: The authors thank D. Spector, L. Sieburth, T. Yu, and the Arabidopsis Biological Resource Center for kindly providing seeds and plasmids. We thank D. Kumar and J. Wang for assistance with mutant screening; S. Goodwin, E. Ghiban, and S. Muller for assisting with the Illumina library preparation and sequencing; L. Liu for assisting with sequence data analysis; T. Mulligan, K. Schlecht, and S. Vermylen for plant care; and members of the Jackson lab for discussion and comments on the manuscript. **Funding:** This research is supported by the National Science Foundation (IOS-1930101) and the Next-Generation BioGreen 21 Program (System & Synthetic Agro-biotech Center, Project No. PJ01322602), Rural Development Administration, Republic of Korea. P.C. was supported by the Cold Spring Harbor Laboratory's Undergraduate Research Program.

Author contributions: M.K. and D.J. conceived of the research and designed experiments; M.K. and P.W. performed RIP qPCR; P.W. performed RNA decay analysis; M.K. and R.B. isolated mutants; P.C. performed PCR-based mapping; M.K. performed all other experiments; D.J. supervised the research activity; M.K. and D.J. analyzed data and wrote the manuscript. All of the authors read and approved the manuscript.

Competing interests: Authors declare no competing interests.

Data and materials availability: All data is available in the main text or the supplementary materials. All materials (seed stocks, plasmids) are available from D. Jackson under a material agreement with Cold Spring Harbor Laboratory.

Supplementary Materials:

Materials and Methods

Figures S1-S9

Tables S1-S2

Movies S1-S4

References (*42-48*)

Figure legends

Fig. 1. AtRRP44A promotes KN1 trafficking. (A-C) The starting line for EMS mutagenesis (A) expresses GFP~GL1~KN1^{c} in mesophyll cells in a *gl1* mutant background, and rescues trichome formation, whereas the *rb31-7* (B) and *mk5-140* (C) mutants lost trichome rescue. Scale bars = 1 mm.

(D-I) Confocal images of a true leaf from the starting trichome rescue line show the accumulation of GFP~GL1~KN1^{c} in both the epidermis (D) and the mesophyll (G), whereas the *rb31-7* and *mk5-140* mutants have a severe reduction of GFP~GL1~KN1^{c} in the epidermis (E and F, respectively) but normal accumulation in the mesophyll (H and I, respectively). Arrows show representative nuclei with GFP~GL1~KN1^{c} fusion protein. White lines show the outlines of epidermal cells. Chlorophyll autofluorescence is shown in magenta. Scale bars = 20 μm. (J) *AtRRP44A* (At2g17510) gene structure, showing different mutant alleles, *atrrp44a-1*, *atrrp44a-4* (*rb31-7*), and *atrrp44a-5* (*mk5-140*). Black bars indicate exons; lines and white boxes represent introns and untranslated regions, respectively. (K) AtRRP44A protein structure, showing different domains and the mutation sites in *atrrp44a-4* and *atrrp44a-5* in the RNB domain. (L and M) *atrrp44a-4* and *atrrp44a-5* mutants rescued by native expression of RFP tagged AtRRP44A have normal trichome rescue (arrows). Scale bars = 1 mm.

Fig. 2. *atrrp44a* mutants enhance *stm* and *cct8* phenotypes. (A-E) Meristem defects in *stm-10* were enhanced by *atrrp44a-4*. *stm-10* mutants had smaller meristems, and the meristem size was even smaller in the *atrrp44a-4; stm-10* double mutants; meristems were shaded in pink. Plants were grown for 14 days under short-day conditions. Bars topped by different letters are significantly different at $P < 0.05$ (Tukey HSD test). Scale bars = 50 μm. (F-H) *atrrp44a-5; cct8-1* double mutants developed enhanced shoot defects. *atrrp44a* and *cct8-1* single mutants had normal shoot development although were slightly shorter than control lines, whereas the *atrrp44a-5; cct8-1* double mutants were severely dwarfed (F, arrowhead) with fasciated stems (G, arrow) and premature termination of the shoot meristem (H, arrow). Scale bars = 1 cm.

Fig. 3. Meristem expression and plasmodesmata localization of AtRRP44A. (A and B) AtRRP44A~RFP (orange) was expressed in the shoot meristem and flower primordia (A), and

epidermal and mesophyll cells in leaf primordia (B). The fusion protein localized in nuclei in all tissues, as shown by co-localization with DAPI (A and B, blue). Scale bars = 50 μm (A, left panels) and 10 μm (A, right panels, and B). (C and D) Some of the AtRRP44A^{NLSA}~NES~RFP protein (orange) was found outside of the nucleus and localized to the periphery of an epidermal cell (C), whereas native AtRRP44A~RFP protein (orange) was detected only in the nucleus (D, asterisks). NLS: nuclear localization signal. NES: nuclear export signal. Scale bars = 20 μm. (E and F) AtRRP44A^{NLSA}~NES~RFP (pink and orange) accumulated in puncta at the boundary between epidermal cells, and co-localized with aniline blue staining of plasmodesmata (E, arrowheads). Scale bars = 10 μm. Quantitative analysis indicated that AtRRP44A accumulated in ~75% of plasmodesmata (F). Orange and blue lines show the fluorescence intensities of RFP and aniline blue along cell-cell boundaries, respectively, and asterisks represent overlaps.

Fig. 4. AtRRP44A mediates KN1 mRNA trafficking. (A-D) To assay KN1 mRNA trafficking, GFP~GL1~KN1^{C}~MBS mRNA and MCP~RFP were expressed in the mesophyll layer and epidermis, respectively (A, epiMCP). In lines WT for *AtRRP44A*, KN1 mRNA trafficked to the epidermis and formed many speckles in the cytoplasm of epidermal cells (B, orange, arrowheads), whereas trafficking was strongly suppressed in *atrrp44a-5* mutants, which had ~ 8 fold fewer epidermal fluorescent puncta compared to WT (C, D). **: $P < 0.01$ (Welch's *t*-test). NLS: nuclear localization signal, MCP: MS2 coat protein, MBS: MS2 bacteriophage binding sequence. Scale bars = 20 μm. (E-H) Co-expression of GFP~GL1~KN1^{C}~MBS mRNA and MCP~RFP in the mesophyll layer (E, mesoMCP) indicated that *atrrp44a-5* mutants had similar numbers of KN1 mRNA puncta in mesophyll cells as in WT (F-H, orange, arrowheads; NS: non-significance [$P = 0.145$, Welch's *t*-test]). Scale bars = 20 μm. Error bars in (D) and (H) denote SD. (I-K) Expression of mesoMCP~RFP significantly reduced trichome rescue compared to epiMCP or lines without MBS/MCP expression (no MCP) (I), and also decreased

405 GFP~GL1~KN1^{c} accumulation in the epidermis (K) in comparison to lines expressing epiMCP~RFP
406 (J). Bars topped by different letters are significantly different at $P < 0.01$ (Tukey HSD test). Arrows
407 point to representative nuclei with GFP~GL1~KN1^{c} fusion protein. Chlorophyll autofluorescence is
408 shown in magenta. White lines show the outlines of epidermal cells. Scale bars = 20 μm. (L)
409 GFP~GL1~KN1^{c}~MBS mRNA (orange, arrowheads) associated with plasmodesmata, as shown by co-
410 localization with aniline blue signals (blue). Scale bar = 10 μm.
411
412
413
414
415
416
417

Figures

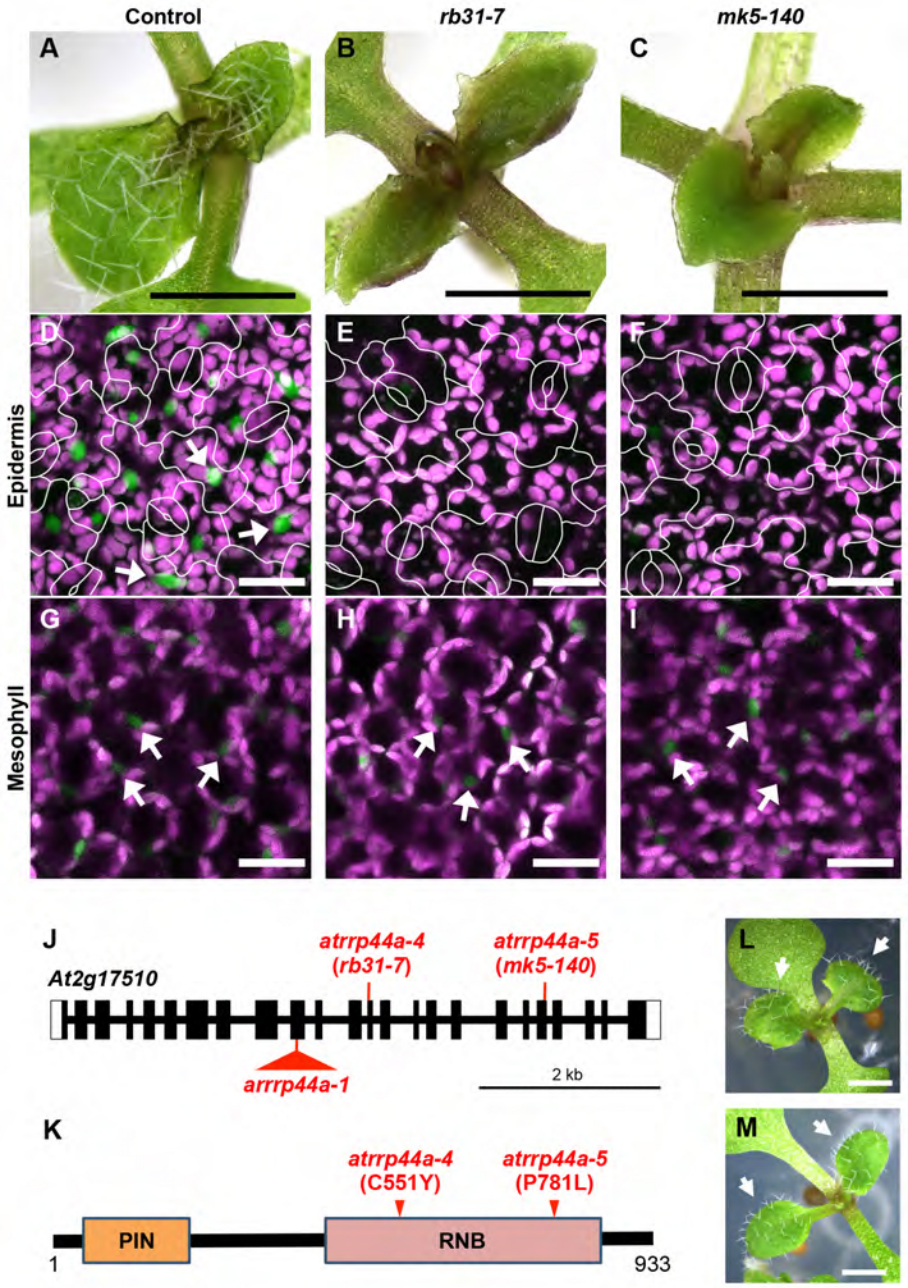

Fig. 1

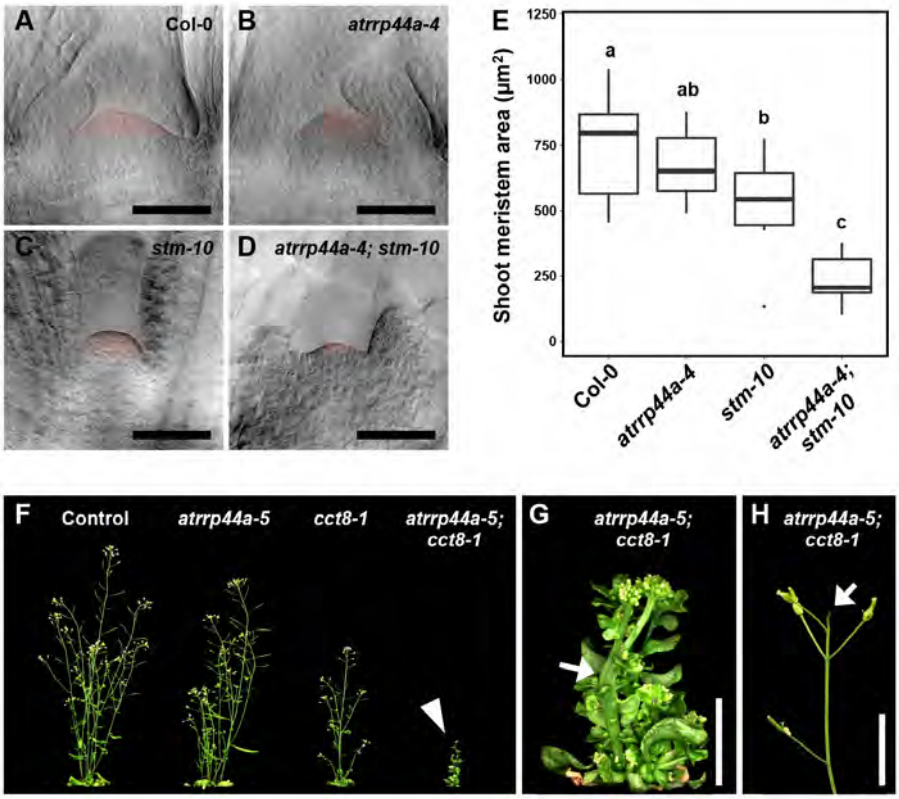
A
Col-0
B
atrrp44a-4
C
stm-10
D
atrrp44a-4; stm-10
E
Shoot meristem area (µm²)
1250
1000
750
500
250
0
a
ab
b
c
Col-0
atrrp44a-4
stm-10
atrrp44a-4; stm-10
F
Control
atrrp44a-5
cct8-1
atrrp44a-5; cct8-1
G
atrrp44a-5; cct8-1
H
atrrp44a-5; cct8-1

Fig. 2

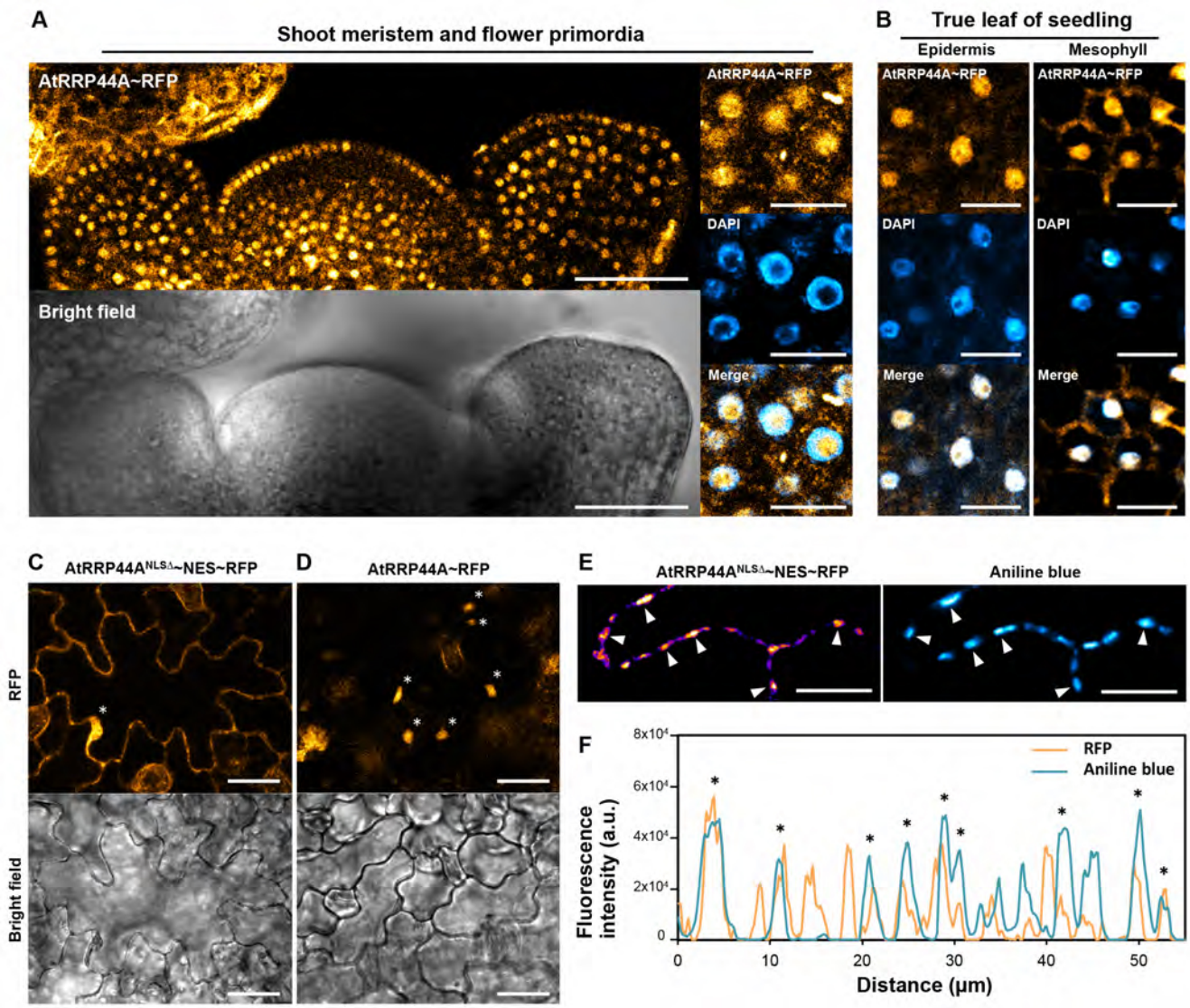
A
Shoot meristem and flower primordia
AtRRP44A~RFP
Bright field
AtRRP44A~RFP
DAPI
Merge
B
True leaf of seedling
Epidermis
Mesophyll
AtRRP44A~RFP
DAPI
Merge
C
AtRRP44A^NLSΔ~NES~RFP
D
AtRRP44A~RFP
RFP
Bright field
E
AtRRP44A^NLSΔ~NES~RFP
Aniline blue
F
RFP
Aniline blue
Fluorescence intensity (a.u.)
8x10⁴
6x10⁴
4x10⁴
2x10⁴
0
0
10
20
30
40
50
Distance (μm)

Fig. 3

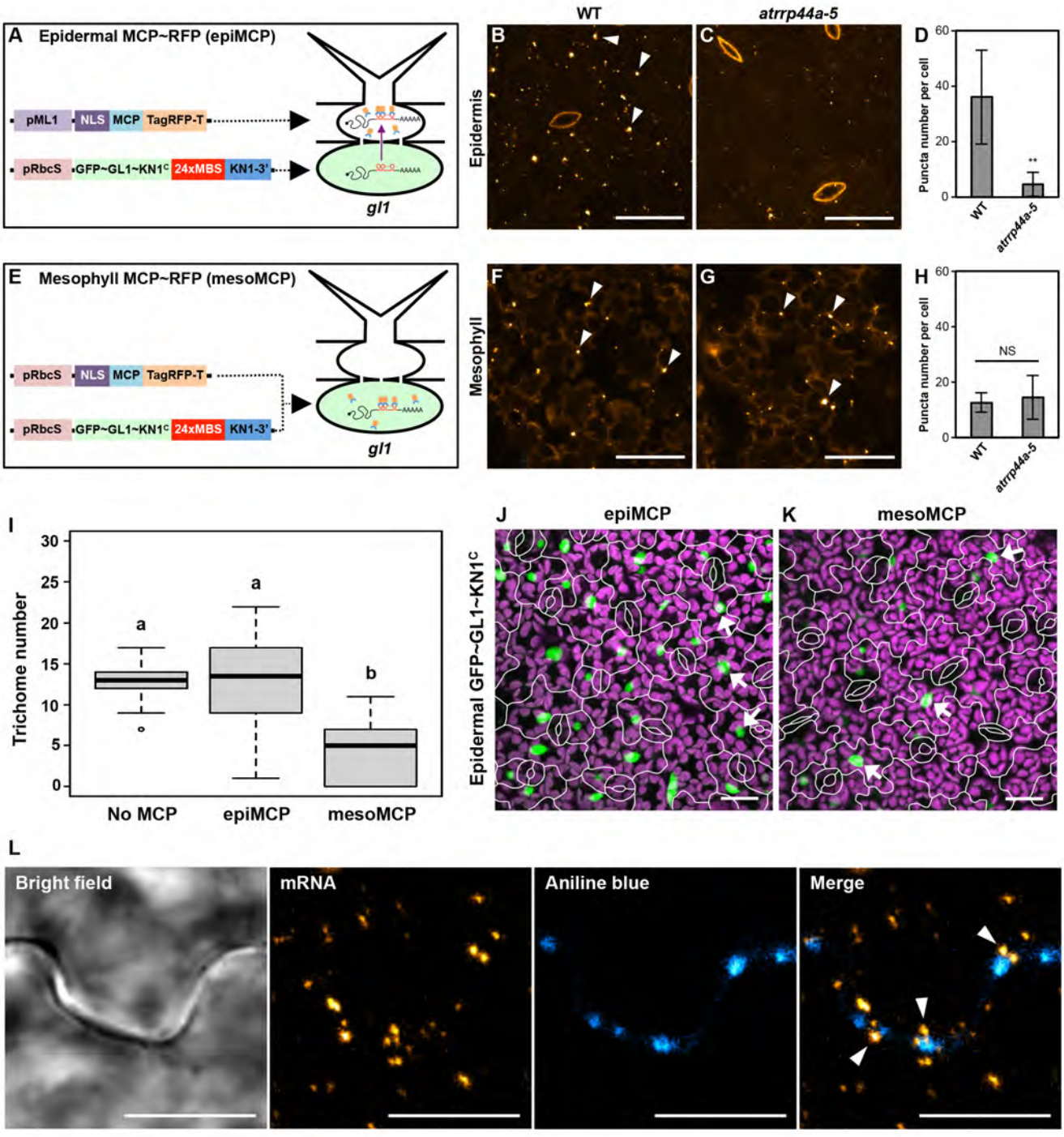
A Epidermal MCP~RFP (epiMCP)
pML1 NLS MCP TagRFP-T
pRbcS GFP~GL1~KN1C 24xMBS KN1-3'
gl1
WT
atrrp44a-5
B
C
Epidermis
D
Puncta number per cell
60
40
20
0
**
WT
atrrp44a-5
E Mesophyll MCP~RFP (mesoMCP)
pRbcS NLS MCP TagRFP-T
pRbcS GFP~GL1~KN1C 24xMBS KN1-3'
gl1
F
G
Mesophyll
H
Puncta number per cell
NS
I
Trichome number
30
25
20
15
10
5
0
a
a
b
No MCP
epiMCP
mesoMCP
J epiMCP
K mesoMCP
Epidermal GFP~GL1~KN1C
L
Bright field
mRNA
Aniline blue
Merge

Fig. 4

Supplementary Materials for

An RNA exosome subunit mediates cell-to-cell trafficking of a homeobox mRNA via plasmodesmata

Munenori Kitagawa, Peipei Wu, Rachappa Balkunde, Patrick Cunniff, and David Jackson*.

*Correspondence to: jacksond@cshl.edu

This PDF file includes:

Materials and Methods
Figs. S1 to S9
Tables S1 to S2
Captions for Movies S1 to S4
References (*42-48*)

Other Supplementary Materials for this manuscript include the following:

Movies S1 to S4

Materials and Methods

Plant materials

Arabidopsis plants were grown on soil or Murashige and Skoog (MS) agar plates under standard long-day or short-day conditions. Trichome rescue lines, *cct8-1*, and *stm-10* were described previously (*7, 31*). *atrrp44a-1* (*17*) is a T-DNA insertion mutant (SALK_037533C) obtained from the Arabidopsis Biological Resource Center (http://www.arabidopsis.org/). All lines were in the Col-0 background. *atrrp44a-4/+; gl1*, *atrrp44a-5/+; gl1*, *atrrp44a-4; stm-10*, *atrrp44a-5; stm-10, atrrp44a-4; cct8-1, and atrrp44a-5; cct8-1* double mutants were generated through genetic crosses, and identified in the F2 segregating populations. *atrrp44a-4* or *-5/ atrrp44a-1* trans-heterozygous plants were generated through genetic crosses, and identified in the F1 segregating populations. *atrrp44a-1, atrrp44a-4*, *atrrp44a-5*, *cct8-1*, and *stm-10* were validated by PCR genotyping with primers listed in table S1. The phenotypes of *atrrp44a; cct8-1* double mutants were examined in plants grown for 36 days under long-day condition. Plant transformation was done by Agrobacterium-mediated floral dip (*42, 43*). Transient protein expression in *Nicotiana benthamiana* leaves was performed as described previously (*44*).

Mutagenesis, mutant screening, and whole-genome mutation analysis

For mutagenesis, seeds of trichome rescue lines were incubated with 100 mM EMS in H_2O for 3-5 hours, then rinsed in H_2O eight times, and planted on soil. M2 seeds were harvested from individual M1 plants, and ~100 M2 seeds per M1 plant were sown on MS agar plates. The first or second true leaves of 7-10-day-old M2 seedlings were observed under a dissecting microscope, and mutants that did not have trichomes were selected as candidate KN1 trafficking defective mutants. Subsequently, GFP~GL1~$KN1^c$ accumulation in the epidermis of the mutant candidates was assessed by confocal laser scanning microscopy (see Materials and Methods, Microscopy) to confirm the defect of GFP~GL1~$KN1^c$ trafficking from the mesophyll to the epidermis. Two mutants that lacked trichomes

and GFP~GL1~KN1^{c} accumulation in the epidermis, *rb31-7* and *mk5-140*, were thus isolated as KN1 trafficking mutants. For preparing mapping populations, selfed heterozygous mutants from M2 families were used to collect M3 non-mutant (*rb31-7*: 74 plants, *mk5-140*: ~100 plants) or mutant pools (*rb31-7*: 33 plants, *mk5-140*: ~100 plants). Genomic DNAs were extracted by a urea based extraction method (*45*) and sequenced using the NextSeq Mid-Output (Illumina Inc., San Diego, CA, USA; read length: 2 x 75 bp, output: 16.25-19.5 Gb, coverage: ~44x). The causal SNPs for *rb31-7* and *mk5-140* were identified by following the MutMap+ pipeline (*15*) (http://genome-e.ibrc.or.jp/home/bioinformatics-team/mutmap) and confirmed by PCR-based fine mapping.

RT-qPCR

The tips of vegetative (~3 mm) or inflorescence shoots (~5 mm) were collected for RNA isolation. Expanded leaves or flowers were carefully removed from shoots. Total RNA was extracted using Direct-zol RNA MiniPrep plus (Zymo Research, Irvine, CA, USA) and first-strand cDNA was synthesized following the SuperScript IV First-Strand Synthesis System (Thermo Fisher Scientific, Waltham, MA, USA). RT-qPCR was performed using KAPA SYBR FAST qPCR Master Mix (2x) Universal (KAPA Biosystems Inc., Wilmington, MA, USA). The transcript levels were normalized against *ACTIN2* (*ACT2*) gene (At3g18780). The data were collected from three (fig. S4F and fig. S7, B and C [*atrrp44a-4* and *atrrp44a-5*]) or six (Fig. S7, B and C [control]) independent biological replicates. RT-qPCR primers used for STM (Fig. S7A), WUSCHEL (WUS), CLAVATA3 (CLV3), and ACT2 are listed in table S1.

mRNA decay analysis

mRNA decay assays were performed as described previously (*16*). Seedlings of control lines and *atrrp44a-5* were cultured with aeration for seven days in MS liquid medium, preincubated in incubation buffer (15 mM sucrose, 1 mM piperazine-N,N'-bis(2-ethanesulfonic acid) (pipes), pH 6.25, 1 mM KCl, 1 mM sodium citrate) with aeration for 30 min, and then supplied with cordycepin (Sigma-Aldrich, MO, USA) to a final concentration of 1 mM. Samples were collected before cordycepin treatment (0 min), and 120 min and 240 min after cordycepin addition. Tissues were flash-frozen in liquid nitrogen just after sampling and stored at -80°C. Total RNA was isolated using Direct-zol RNA MiniPrep plus kit (Zymo Research), and cDNA was synthesized using random hexamers using SuperScript III First-Strand Synthesis System (Thermo Fisher Scientific). STM mRNA levels in each sample were quantified by RT-qPCR using KAPA SYBR FAST qPCR Master Mix (2x) Universal (KAPA Biosystems Inc.). The data were collected from three independent biological replicates with three technical replicates. Transcript abundance was expressed as a ratio relative to the time 0 sample for RNA decay. RT-qPCR primers used for STM mRNA decay analysis (RNAdecay-STM_F and R) (Fig. S7A) are listed in table S1.

RNA-immunoprecipitation (RIP) qPCR

For AtRRP44A RIP, the tips of inflorescence shoots of *pAtRRP44A::AtRRP44A~RFP; atrrp44a-1* and Col-0 (negative control) were used. Tissues were collected and vacuum-infiltrated with 1% formaldehyde (Electron Microscopy Sciences, PA, USA) in PBS for 15 min, followed by quenching with 125 mM glycine in PBS. Extracts were prepared in lysis buffer (50 mM Tris-HCl pH 7.5, 150 mM NaCl, 4 mM $MgCl_2$, 0.25% Igepal CA-630, 0.1% SDS, 50 μg/mL Heparin, 1 mM DTT, 130 μM Bortezomib, 1 mM Phenylmethylsulfonyl fluoride, 10 mM Sodium Fluoride, 40 U/ml RNaseOUT (Invitrogen, Carlsbad, CA, USA), and Complete Protease Inhibitor). The extract was incubated for 10 min with rotating at 4°C, pre-cleared by centrifugation (16,300g for 10 min). The immunoprecipitations (IPs) of AtRRP44A~RFP and the negative control (Col-0 extract) were

97 performed with RFP-Trap Magnetic Agarose (MA) beads (Chromotek, Planegg, Germany; Product
98 code: rtma, RRID: AB_2631363) for two hours. The beads were washed three times with lysis buffer.
99 RNAs in the input and RIP samples were isolated by TRI Reagent (Zymo Research) and RNA Clean &
100 Concentrator-5 kit (Zymo Research). RNAs were reverse transcribed with random hexamers using
101 SuperScript IV First-Strand Synthesis System (Thermo Fisher Scientific). STM and UBIQUITIN 7
102 (UBQ7, a negative control gene) mRNA levels in each sample were quantified by RT-qPCR using
103 KAPA SYBR FAST qPCR Master Mix (2x) Universal (KAPA Biosystems Inc.). Relative enrichment
104 of STM and UBQ7 was calculated by ΔΔCt method. Ct values of RIP samples were normalized to that
105 of the input samples, and then normalized to the values of negative controls (Col-0 extract, RFP-trap
106 MA beads IP). The data were collected from three independent biological replicates with a minimum of
107 two technical replicates. RIP-qPCR primers used for STM (RIP-STM_F and R, Fig. S7A) and UBQ7
108 are listed in table S1.
109

110 **Microscopy**

111 Seedling images were taken with a Nikon SMZ1500 (Nikon Instruments Inc., Melville, NY, USA)
112 microscope to manually capture Z series, which were then merged using NIS-Elements BR 3.2 imaging
113 software (Nikon Instruments Inc.) to create focused images.

114 Confocal images were obtained on a ZEISS LSM710 or LSM 900 microscope (Carl Zeiss,
115 Oberkochen, Germany). For all observations except the inflorescence meristem and flower primordia,
116 the first or second true leaves (1-2 mm length) of 7- or 10-day-old seedlings, respectively, were used.
117 The GFP observations in trichome rescue, epiMCP, and mesoMCP lines were performed by Z-stack
118 imaging (Pinhole = 1 airy unit [~0.6 μm section], interval = 1.5 μm). The signals of GFP and
119 chlorophyll A were scanned from the epidermis to mesophyll cell layers. Autofluorescence of
120 chloroplasts was also detected in the GFP channel, and was distinguished from the true GFP signal by

comparison with the chlorophyll A signal. The observations of RFP fluorescence puncta in the epidermis and mesophyll cell layer of the epiMCP and mesoMCP lines, respectively, were performed by Z-stack imaging (Pinhole = 1 airy unit [~0.6 μm section], interval = 1 μm). For observing co-localization of AtRRP44A^{NLSA}~NES~RFP or MCP~RFP fluorescent puncta with plasmodesmata, dissected true leaves of each transformant were stained with aniline blue just before observation (see Materials and Methods, Aniline blue staining). The time-lapse imaging was performed with 15 or 30 seconds intervals. For observing AtRRP44A~RFP in the inflorescence meristem and flower primordia, dissected inflorescence apices of *pAtRRP44A::AtRRP44A~RFP; atrrp44a-1* lines were embedded in 6% agar blocks, and sections were obtained using a vibratome and stained with DAPI just before observation. For leaf primordia of these lines, ~1 mm true leaves of seedlings were dissected and stained with DAPI on a slide immediately before observation.

The excitation and emission spectra used for detecting each fluorophore are shown in table S2.

Image analysis

Image files from the confocal microscope were processed using ImageJ-Fiji software (ImageJ; https://imagej.net/Fiji). To show GFP fluorescence, chlorophyll autofluorescence and RFP fluorescent puncta images in Fig. 1, Fig. 4, fig. S3, fig. S7, and fig. S8, five optical sections from the Z-stack images of the epidermis or mesophyll layer were integrated using the Sum Slices tool. For the quantification of nuclear GFP fluorescence, the ROI surrounding the nucleus as estimated by the GFP signal was set and the mean fluorescence intensity inside the ROI was measured by Measure tool in an optical section. The fluorescence signal of a nearby empty region was measured as background, and was subtracted from the GFP signal to calculate the net intensity of GFP.

For analyzing the co-localization of AtRRP44A^{NLSA}~NES~RFP and aniline blue signals in cell walls, the fluorescence intensity of RFP images was adjusted so that the fluorescence intensity of empty regions on the cell wall was close to zero. RFP and aniline blue images were then denoised by

the Despeckle tool. A line selection was then set for a cell wall (83-148 μm) using the segmented line tool, and the Plot Profile tool was used to quantify the fluorescence intensities of RFP and aniline blue depending on the position along the wall. The total number of peaks in the aniline blue signal was then called as the number of plasmodesmata, and peaks that overlapped with the RFP peaks were determined as plasmodesmata with AtRRP44A accumulation. 302 plasmodesmata from 10 cells were analyzed.

The number of RFP fluorescence puncta per cell in epiMCP and mesoMCP lines was counted manually using the cell counter tool. We examined 40 epidermal cells from three independent transgenic lines for each of the epiMCP WT and epiMCP *atrrp44a-5* lines, and 46 mesophyll cells from two independent transgenic lines for each of the mesoMCP WT and mesoMCP *atrrp44a-5* lines. The size of RFP fluorescence puncta in the epidermis of the epiMCP WT and epiMCP *atrrp44a-5* lines was measured using the Analyze Particles tool. First, the areas of fluorescence puncta were estimated by setting a threshold using the Threshold tool, and then the area (pixel number) of each punctum was quantified by the Analyze Particle tool. The puncta with more than two pixels were used for the analysis. We analyzed 189 puncta for epiMCP WT lines and 148 puncta for epiMCP *atrrp44a-5* lines.

Aniline blue staining

Callose staining with aniline blue was performed as described previously (*46*). Aniline blue was dissolved in 10 mM K_3PO_4 (pH 12) to a concentration of 0.01% (w/v). The aniline blue solution was incubated in the dark for more than two days, and the change of the color from blue to yellow was confirmed. This working solution was added to samples just before observation.

mRNA *in situ* hybridization

mRNA *in situ* hybridization was performed as described previously (*47*). Briefly, Col-0 and *atrrp44a; stm-10* plants grown for four weeks under short-day conditions were collected, and fixed in ice-cold

FAA solution (3.8% formalin, 5% acetic acid, 50% ethanol). The fixed tissue was dehydrated through a graded alcohol series (70%, 85%, 95%, and 100%) and a histoclear series, then embedded in paraplast (McCormick Scientific, MO, USA). 10 mm sections were cut using a Leica microtome, then mounted on Probe On Plus Slides (Fisher Scientific, NH, USA). Antisense RNAs for *STM*, *CLV3*, and *WUS* were transcribed by *in vitro* transcription using T7 RNA Polymerase (Sigma-Aldrich) and used as probes. The primers used to prepare the probes are listed in Table S1. Probes were applied on tissue sections and hybridized at 50°C overnight. NBT/BCIP Ready-to-Use Tablets (Roche, Basel, Switzerland) were freshly dissolved in water and used to detect the hybridization signal. Images were taken using a DS-Ri2 DIC microscope (Nikon) and were representative of at least two independent biological replicates for each probe and genotype.

Shoot meristem size measurement

Shoot meristem size measurement was performed as described previously (*30*). Briefly, seedlings grown for 14 days under short-day conditions were harvested and then fixed overnight in ice-cold FAA (10% formalin, 45% ethanol and 5% acetic acid) followed by dehydration through an ethanol series, and cleared with methyl salicylate (Sigma-Aldrich, St. Louis, MO, USA). Meristems were observed with Nomarski optics using a DS-Ri2 DIC microscope (Nikon). With ImageJ-Fiji, ROIs were set for the shoot meristems (red shaded regions in Fig. 2, A-D and fig. S4G) and their areas were quantified. The data were collected from 7-14 plants for each genotype.

Molecular biology

pAtRRP44A::AtRRP44A~RFP vector

The p35S::AtRRP44A~ECFP vector (*16*) was kindly provided by Dr. Leslie Sieburth. The 35S promoter and ECFP coding sequence were replaced by the native promoter of AtRRP44A and TagRFP-T coding sequence. The AtRRP44A promoter fragment was amplified from genomic DNA by PCR with primers MK1 and MK2 (table S1), and the whole region except 35S promoter of p35S::AtRRP44A~ECFP vector was amplified by PCR with primers MK3 and MK4 (table S1). These two fragments were ligated according to the manufacturer's directions of InFusion HD Cloning Kit (Takara Bio, Ohtsu, Japan) to generate pAtRRP44A::AtRRP44A~ECFP. Then, the whole vector except ECFP was amplified by PCR with primers MK5 and MK6 (table S1), and the TagRFP-T coding region was PCR-amplified from a pDONR clone containing TagRFP-T with primers MK7 and MK8 (table S1). These two fragments were ligated by InFusion HD Cloning Kit to generate the pAtRRP44A::AtRRP44A~RFP vector. This vector was transformed into *rb31-7*, *mk5-140*, or *atrrp44a-1*/+ plants. Transgenic plants were screened by Basta selection.

pAtRRP44A::AtRRP44A^{NLSA}~NES~RFP vector

To insert a NES sequence between AtRRP44A and TagRFP-T coding regions in the pAtRRP44A::AtRRP44A~RFP, the vector was linearized by PCR using primers MK9 and MK10 (table S1) that contain NES coding sequence (*48*), and the vector was self-ligated by InFusion HD Cloning to generate pAtRRP44A::AtRRP44A~NES~RFP. For deleting the two native NLSs in AtRRP44A, they were first predicted by the SeqNLS prediction tool (http://mleg.cse.sc.edu/seqNLS/). The pAtRRP44A::AtRRP44A~NES~RFP vector was linearized by PCR using primers MK11 and MK12 (table S1) that have mutations for deleting the first NLS. After self-ligation by InFusion HD Cloning Kit, the vector was linearized again by PCR using primers MK13 and MK14 (table S1) that contain mutations for deleting the second NLS. This linearized vector was self-ligated by InFusion HD Cloning Kit to generate the pAtRRP44A::AtRRP44A^{NLSA}~NES~RFP vector. This vector was transformed into Col-0 plants. Transgenic plants were screened by Basta selection.

pRbcS::GFP~GL1~KN1^{c}~MBS vector and pML1 or pRbcS::NLS~MCP~RFP vectors

For pRbcS::GFP~GL1~KN1^{c}~MBS vector, the 24 repeats of the MBS were inserted between the stop codon and KN1 3'UTR in the pRbcS::GFP~GL1~KN1^{c} vector (*7*). For this, the pRbcS::GFP~GL1~KN1^{c} vector was linearized by PCR with primers MK15 and MK16 (table S1). The 24 repeats of MBS were cut from the pCR4-24XMS2SL-stable vector (Addgene plasmid # 31865) using *Not*I and *Bgl*II, and ligated into the linearized vector using InFusion HD Cloning Kit to generate pRbcS::GFP~GL1~KN1^{c}~MBS vector.

For pML1 or pRbcS::NLS~MCP~RFP, the MCP coding region was PCR-amplified from the pMS2-YFP vector (Addgene plasmid # 27122) with primer MK17 that contains the NLS from the Arabidopsis *FD* gene (At4g35900) (*41*), and primer MK18 (table S1). The FD NLS targets the fusion protein into the nucleus to reduce the background cytoplasmic signal (*41*). The TagRFP-T coding region was PCR-amplified from a pDONR clone containing TagRFP-T using primers MK19 and MK20 (table S1). Using MCP and TagRFP-T fragments, an NLS~MCP~TagRFP-T fragment was amplified by an overlap extension PCR with primers MK17 and MK20, and cloned into pCR-Blunt II-TOPO vector (Invitrogen, Carlsbad, CA, USA). The NLS~MCP~TagRFP-T coding region was cut from the pCR-NLS~MCP~TagRFP-T vector by *Xho*I digestion, and ligated by Rapid Ligation DNA kit (Thermo Fisher Scientific) into binary vectors containing pML1 or pRbcS to generate pML1::NLS~MCP~RFP and pRbcS::NLS~MCP~RFP vectors. pCR4-24XMS2SL-stable and pMS2-YFP vectors were kindly provided by Dr. David Spector. The pRbcS::GFP~GL1~KN1^{c}~MBS vector and pML1 (or pRbcS)::NLS~MCP~RFP vectors were transformed together into *atrrp44a-4*/+*; gl1* and *atrrp44a-5*/+*; gl1* mutants as previously described (*43*). The transgenic plants were screened by hygromycin selection to obtain pRbcS::GFP~GL1~KN1^{c}~MBS positive plants, and in turn, pML1 (or pRbcS)::NLS~MCP~RFP positive plants were screened by fluorescent microscopy screening. Finally, T1 plants that possessed both constructs in *atrrp44a-4*/+*; gl1* or *atrrp44a-5*/+*; gl1* were isolated, and the cell-to-cell trafficking of KN1 mRNA was assayed in T2 generation *atrrp44a* homozygotes or non-mutant sibling (WT) control lines.

pRbcS::GFP~GL1~STM^{c} vector

KN1^{c} coding and 3' UTR regions in the pRbcS::GFP~GL1~KN1^{c} vector were replaced with those of STM. The C-terminal region of STM (STM$^{276\text{-}382}$) which is the homologous region to KN1^{c} (*7, 13*) was used as the STM^{c}. First, STM^{c} coding was PCR-amplified from a STM cDNA clone using primers MK21 and MK22 (STM^{c}), and a region of ~850 bp behind the stop codon of the *STM* gene was PCR-amplified from an STM genomic clone using primers MK23 and MK24 (STM 3' UTR). Next, the pRbcS::GFP~GL1~KN1^{c} vector was digested with *Sal*I to remove KN1^{c} coding and KN1 3' UTR. Then, this digested vector and STM^{c}, STM 3' UTR fragments were ligated using ClonExpress MultiS One Step Cloning kit (Vazyme, Nanjing, China) to generate the pRbcS::GFP~GL1~STM^{c} vector. This vector was transformed into *atrrp44a-5/+; gl1* plants. Transgenic plants were screened by hygromycin selection. Trichome rescue assays were performed in the T1 generation.

pAtRRP44A::AtRRP44A^{D489N}~RFP vector

To generate non-catalytic AtRRP44A, Asp489 was substituted to Asn as described previously (AtRRP44A^{D489N}) (*27*). The pAtRRP44A::AtRRP44A~RFP vector was linearized by PCR using primers MK25 and MK26 (table S1) that have mutations for D489N substitution. This linearized vector was self-ligated by ClonExpress II One Step Cloning kit (Vazyme) to generate the pAtRRP44A::AtRRP44A^{D489N}~RFP vector. This vector was transformed into *atrrp44a-5; pRbcS::GFP~GL1~KN1^{c}* plants. Transgenic plants were screened by Basta selection. Trichome rescue assays were performed in the T1 generation.

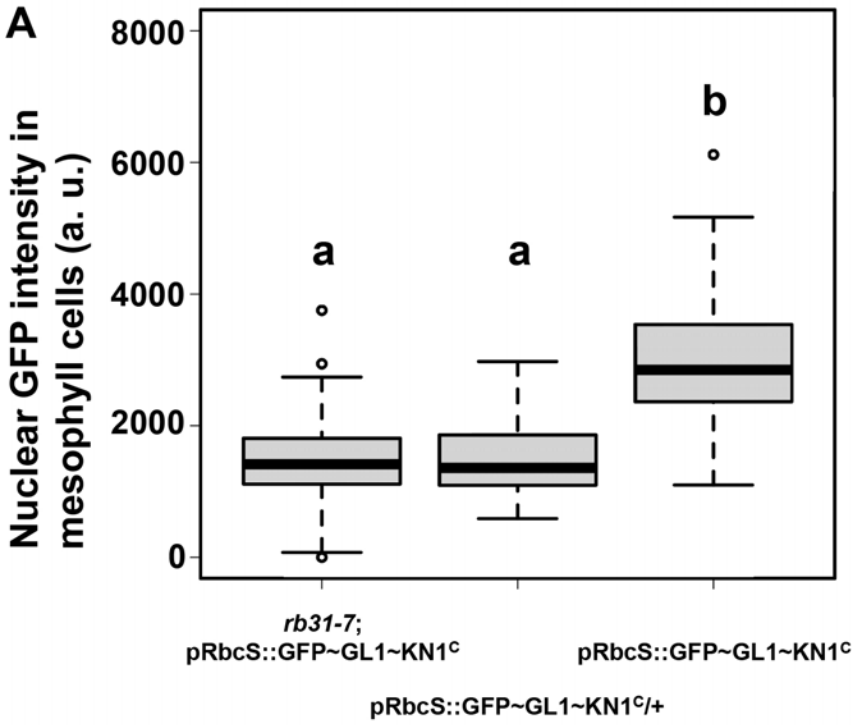
A
Nuclear GFP intensity in mesophyll cells (a. u.)
8000
6000
4000
2000
0
a
a
b
rb31-7; pRbcS::GFP~GL1~KN1C
pRbcS::GFP~GL1~KN1C
pRbcS::GFP~GL1~KN1C/+

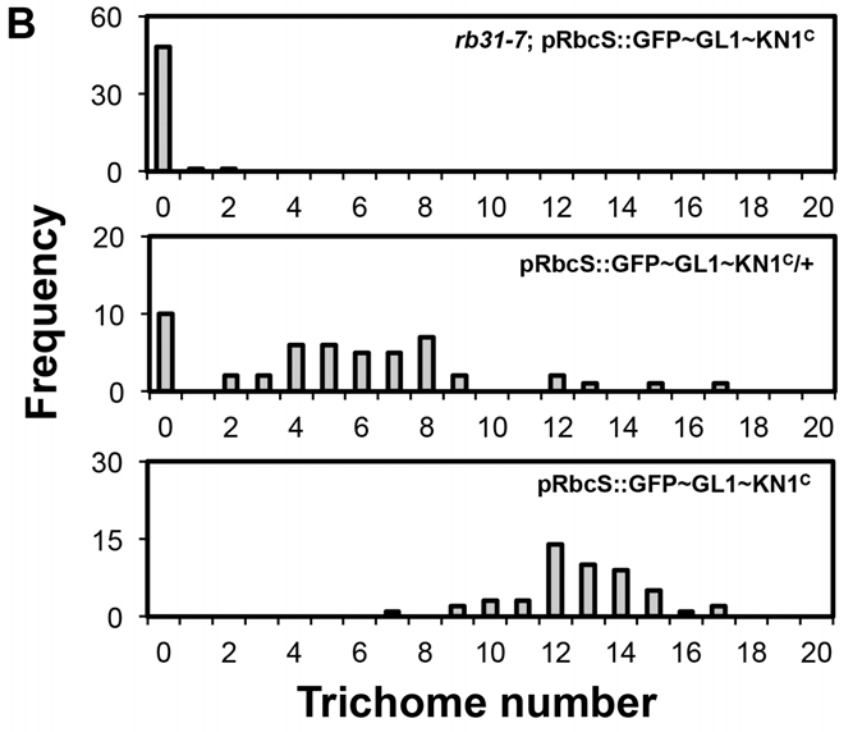
B
rb31-7; pRbcS::GFP~GL1~KN1C
pRbcS::GFP~GL1~KN1C/+
pRbcS::GFP~GL1~KN1C
Frequency
Trichome number

Fig. S1. Reduced GFP~GL1~KN1^{c} expression in hemizygous trichome rescue lines is sufficient for trichome rescue. (A) Nuclear GFP intensity in mesophyll cells of *rb31-7* mutants and the *pRbcS::GFP~GL1~KN1^{c}* hemizygous plants was ~ half that of the control lines (n= 34-61). Bars topped by different letters are significantly different at $P < 0.01$ (Tukey HSD test). GFP intensity of 10-13 mesophyll nuclei in the first or second leaves was measured in five *rb31-7* mutant plants, six homozygous or three hemizygous trichome rescue transgene plants. (B) *rb31-7* mutants rarely formed trichomes, whereas *pRbcS::GFP~GL1~KN1^{c}* hemizygous plants rescued trichome formation, with trichome numbers ~ half of that of the homozygous trichome rescue transgene plants. For quantifying trichome numbers, 50-54 plants were assayed for each genotype.

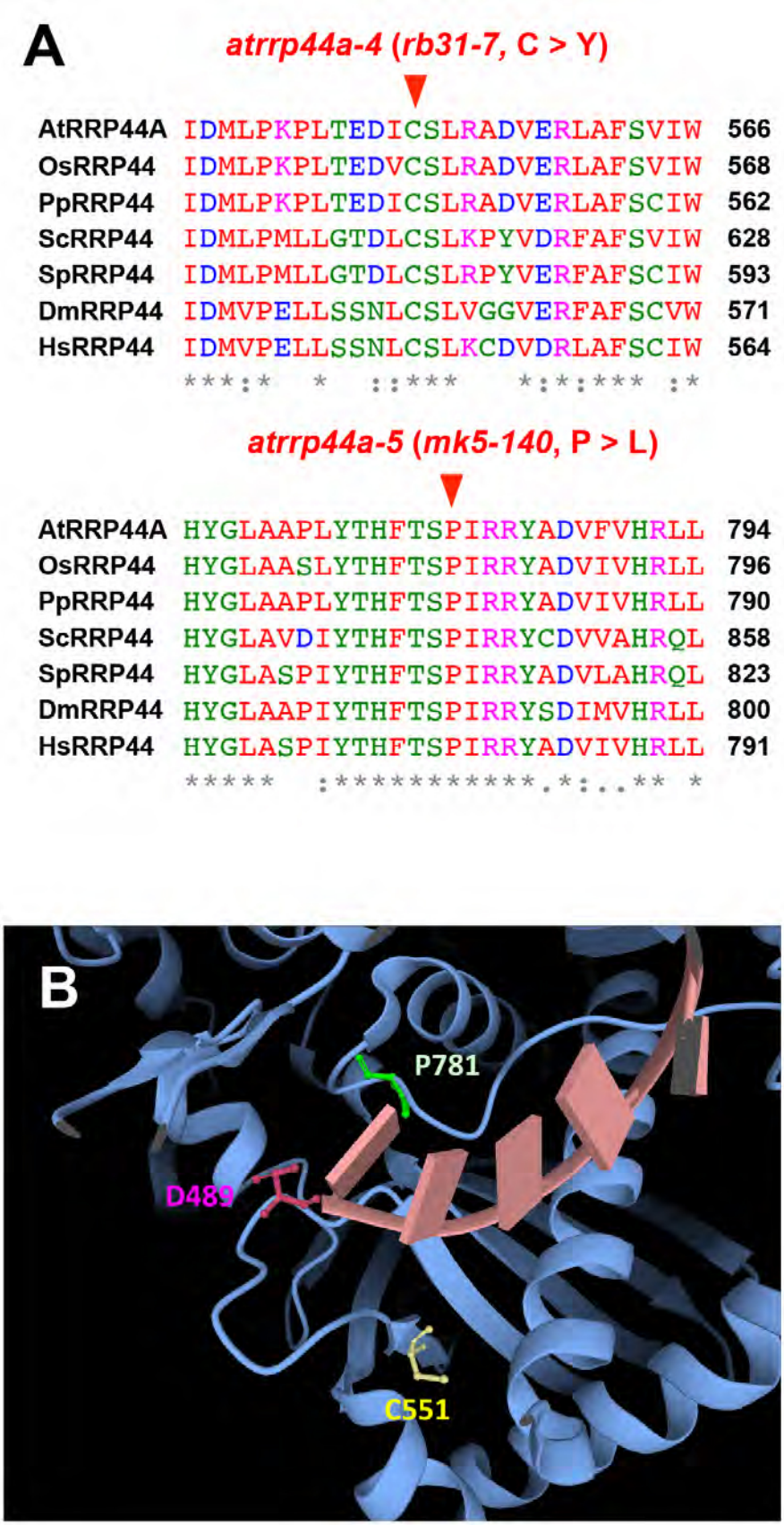
A
atrrp44a-4 (rb31-7, C > Y)
AtRRP44A IDMLPKPLTEDICSLRADVERLAFSVIW 566
OsRRP44 IDMLPKPLTEDVCSLRADVERLAFSVIW 568
PpRRP44 IDMLPKPLTEDICSLRADVERLAFSCIW 562
ScRRP44 IDMLPMLLGTDLCSLKPYVDRFAFSVIW 628
SpRRP44 IDMLPMLLGTDLCSLRPYVERFAFSCIW 593
DmRRP44 IDMVPELLSSNLCSLVGGVERFAFSCVW 571
HsRRP44 IDMVPELLSSNLCSLKCDVDRLAFSCIW 564
atrrp44a-5 (mk5-140, P > L)
AtRRP44A HYGLAAPLYTHFTSPIRRYADVFVHRLL 794
OsRRP44 HYGLAASLYTHFTSPIRRYADVIVHRLL 796
PpRRP44 HYGLAAPLYTHFTSPIRRYADVIVHRLL 790
ScRRP44 HYGLAVDIYTHFTSPIRRYCDVVAHRQL 858
SpRRP44 HYGLASPIYTHFTSPIRRYADVLAHRQL 823
DmRRP44 HYGLAAPIYTHFTSPIRRYSDIMVHRLL 800
HsRRP44 HYGLASPIYTHFTSPIRRYADVIVHRLL 791
B
P781
D489
C551

278

279

Fig. S2. The mutated amino acid residues in *atrrp44a-4* and *atrrp44a-5* mutants are highly conserved among plants and animals, and in the vicinity of the RRP44 catalytic center. (A) Amino acid sequence alignment of RRP44 from *A. thaliana* (AtRRP44A), *O. sativa* (OsRRP44), *P. patens* (PpRRP44), *S. cerevisiae* (ScRRP44), *S. pombe* (SpRRP44) *D. melanogaster* (DmRRP44), and *H. sapiens* (HsRRP44). The numbers on the right correspond to the position of the last amino acid shown for each sequence. Asterisks show identical amino acids, and similar amino acids are shown by periods or colons. Arrowheads show the mutated residues in *atrrp44a-4* and *atrrp44a-5* mutants. (B) Ribbon diagram representation of *S. cerevisiae* RRP44 (blue, PDB: 4IFD) with residues corresponding to P781 (green) and C551 (yellow) in AtRRP44A marked. The position of AtRRP44A D489, which corresponds to ScRRP44 D551 that is critical for coordinating magnesium ions in the catalytic center of RRP44, is shown in magenta. Single-stranded RNA is shown in pink.

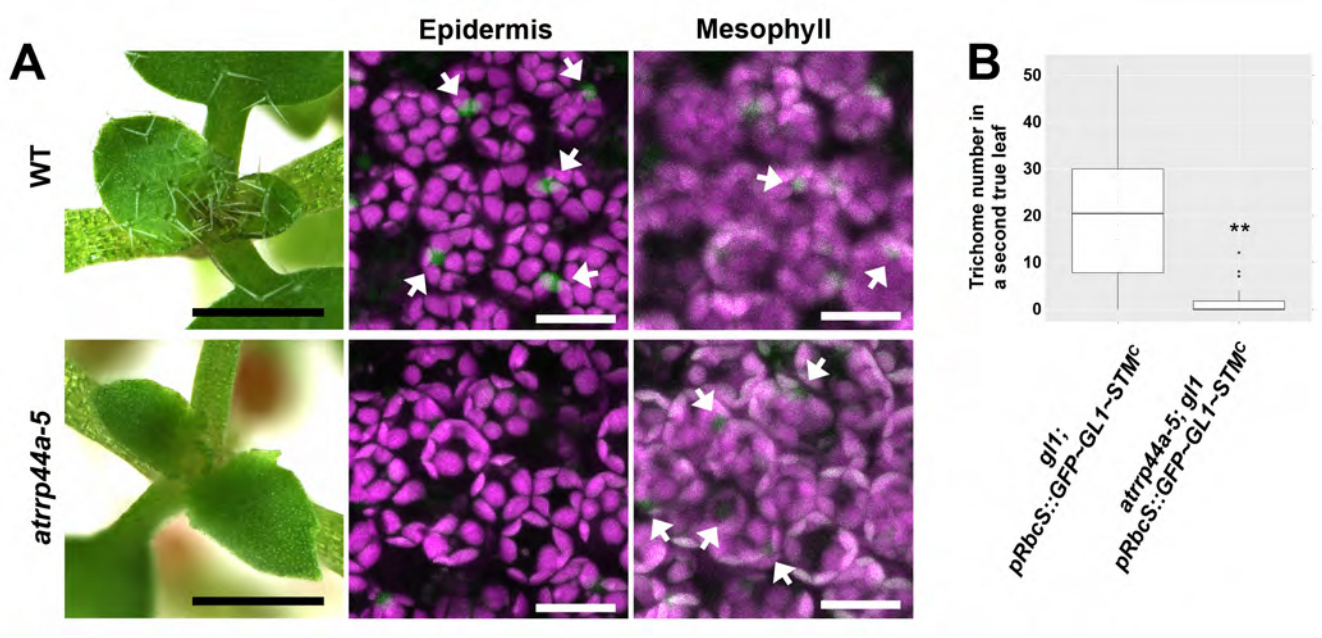

Fig. S3. AtRRP44A mediates STM transport between cells. (A and B) In *pRbcS::GFP~GL1~STM^{c}; gl1* plants, the fusion protein moved from the mesophyll layer to the epidermis and rescued trichome formation in WT plants, but not in *atrrp44a-5* mutants. Scale bars = 1 mm (seedlings) and 20 μm (fluorescent images). Arrows show representative nuclei with GFP~GL1~STM^{c} fusion protein, and chlorophyll autofluorescence is shown in magenta (A). The second true leaves of plants grown for 12 days under long-day conditions were used for the trichome rescue assay. N = >25 plants per line, **: $P < 0.01$ (Welch's *t*-test) (B).

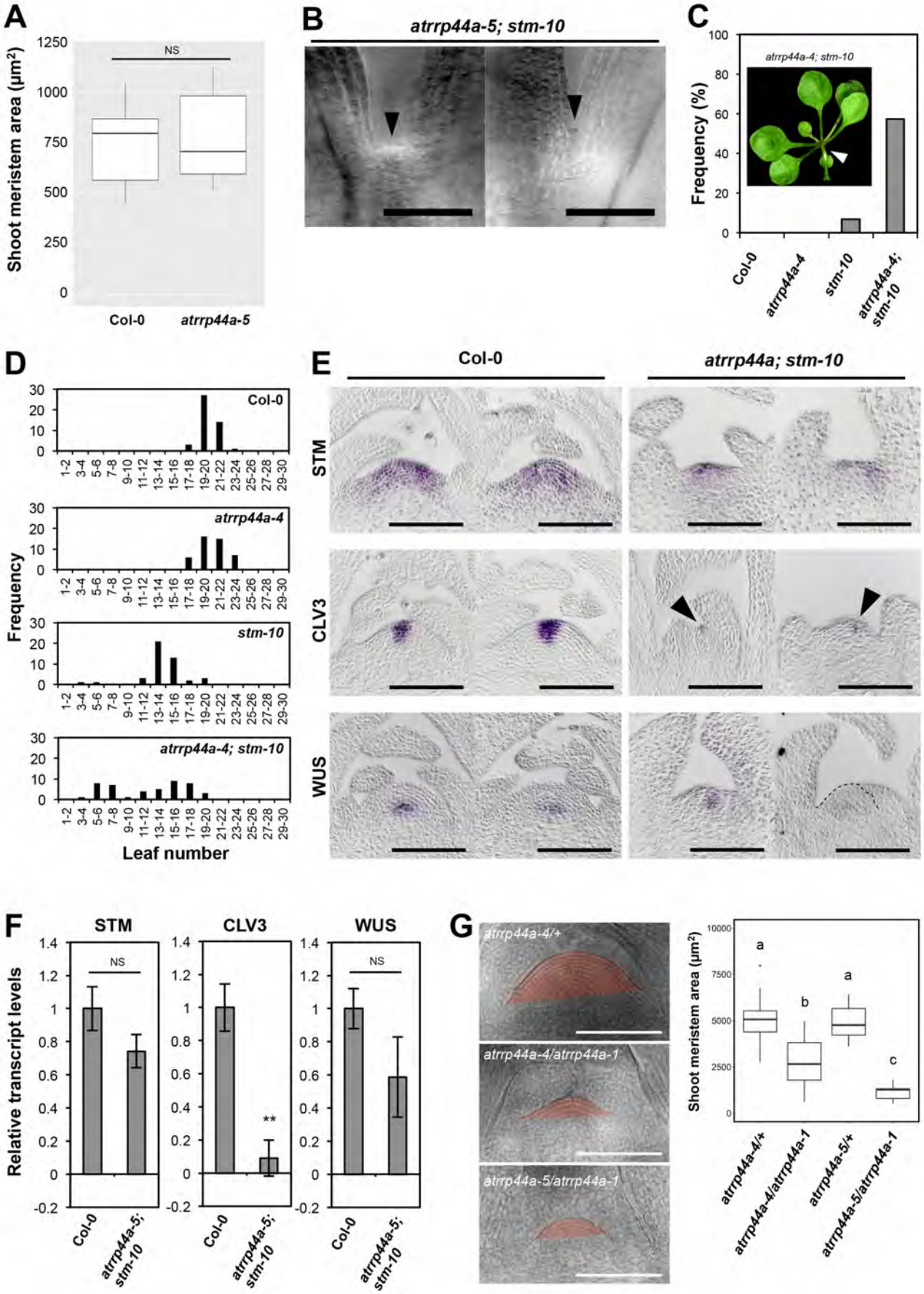
A
Shoot meristem area (µm²)
1250
1000
750
500
250
0
NS
Col-0
atrrp44a-5
B
atrrp44a-5; stm-10
C
Frequency (%)
100
80
60
40
20
0
atrrp44a-4; stm-10
Col-0
atrrp44a-4
stm-10
atrrp44a-4; stm-10
D
Frequency
Col-0
atrrp44a-4
stm-10
atrrp44a-4; stm-10
1-2
3-4
5-6
7-8
9-10
11-12
13-14
15-16
17-18
19-20
21-22
23-24
25-26
27-28
29-30
Leaf number
E
Col-0
atrrp44a; stm-10
STM
CLV3
WUS
F
STM
CLV3
WUS
Relative transcript levels
1.4
1.2
1
0.8
0.6
0.4
0.2
0
-0.2
NS
**
Col-0
atrrp44a-5; stm-10
G
atrrp44a-4/+
atrrp44a-4/atrrp44a-1
atrrp44a-5/atrrp44a-1
Shoot meristem area (µm²)
10000
7500
5000
2500
0
a
b
a
c
atrrp44a-4/+
atrrp44a-4/atrrp44a-1
atrrp44a-5/+
atrrp44a-5/atrrp44a-1

303

Fig. S4. AtRRP44A regulates shoot meristem development through a STM-dependent pathway. (A) *atrrp44a-5* mutants had similar shoot meristem size as in WT. NS: non-significance ($P = 0.584$, Welch's *t*-test). (B) *atrrp44a-5; stm-10* double mutants grown for two weeks under short-day conditions had greatly reduced or abnormal shoot meristems. Arrowheads indicate a shoot meristem (left) and a highly reduced structure (right). Scale bar = 50 μm. (C) *atrrp44a-4; stm-10* double mutants had an increased frequency of plants with shoot meristem arrest. Plants were grown for four weeks under short-day conditions. N = 45-47 plants. Arrowhead indicates shoot meristem termination in *atrrp44a-4; stm-10*. (D) *atrrp44a-4; stm-10* double mutants had fewer leaves (four-week-old plants) under short-day conditions. N = 44-47 plants. (E) mRNA *in situ* hybridization indicated that the expression of *STM*, *CLAVATA3* (*CLV3*), and *WUSCHEL* (*WUS*) (purple) were disorganized and/or reduced in shoot meristems of *atrrp44a; stm-10* double mutants. Arrowheads indicate highly reduced *CLV3* mRNA signal in *atrrp44a; stm-10* double mutants. Scale bar = 100 μm. (F) RT-qPCR indicated that *CLV3* expression was significantly decreased in the *atrrp44a-5; stm-10* double mutants ($P < 0.01$, Welch's *t*-test). Plants were grown for two weeks under short-day conditions. NS: non-significance ($P = 0.059$ [*STM*], $P = 0.078$ [*WUS*]; Welch's *t*-test). (G) *atrrp44a-4 or -5/ atrrp44a-1* (weak allele / null) mutant plants had significantly smaller meristems (shaded in pink). Plants were grown for four weeks under short-day conditions. Bars topped by different letters are significantly different at $P < 0.05$ (Tukey HSD test). Scale bars = 100 μm.

Fig. S5. The *atrrp44a-4; cct8-1* double mutants were defective in shoot development, with fasciated stems and premature meristem termination. (A) *atrrp44a-4* single mutants were slightly shorter than control lines, but did not show other obvious defects in shoot development. By contrast, *atrrp44a-4; cct8-1* double mutants displayed severe defects in shoot development and developed dwarf shoots (arrowhead). This phenotype was never seen in *cct8-1* single mutants. (B) The *atrrp44a-4; cct8-1* double mutants developed fasciated stems (arrow) and premature meristem termination of non-fasciated shoots (arrowhead). Scale bar = 1 cm.

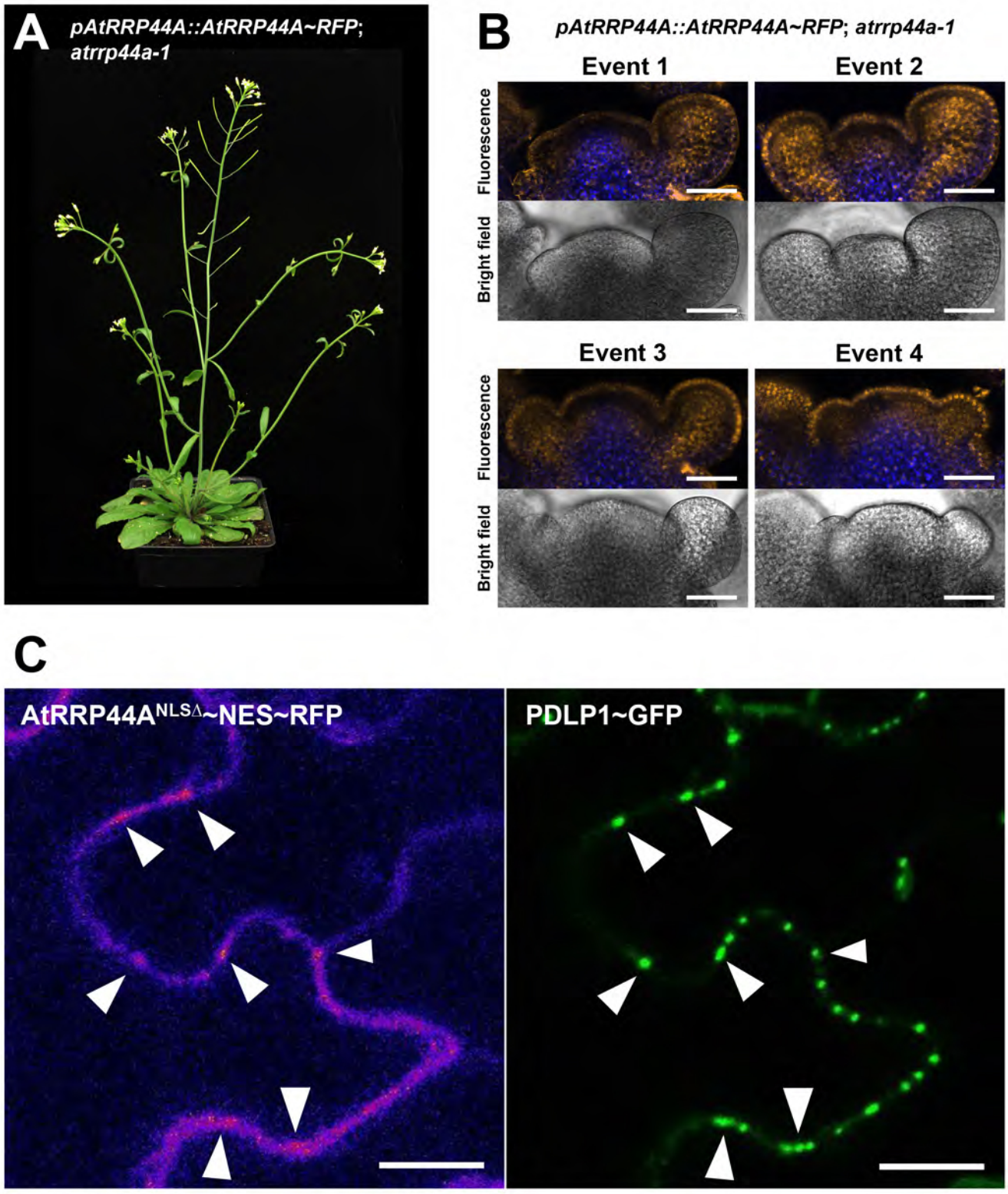

Fig. S6. AtRRP44A is expressed in the shoot meristem and possesses plasmodesmata localization capacity. (A) The *pAtRRP44A::AtRRP44A~RFP* construct fully complemented the *atrrp44a-1* null

mutant. (B) AtRRP44A~RFP (orange) was expressed throughout the shoot meristem in four independent transformants. Blue represents plastids. Scale bar = 50 μm. (C) AtRRP44A^{NLSA}~NES~RFP expressed transiently in tobacco leaves (left panel, pink) co-localized with plasmodesmata labeled by PLASMODESMATA LOCATED PROTEIN1 (PDLP1)~GFP (right panel, green) (arrowheads). NLS: nuclear localization signal, NES: nuclear export signal. RFP signal was shown by Fire LUT in Fiji software. Scale bar = 50 μm.

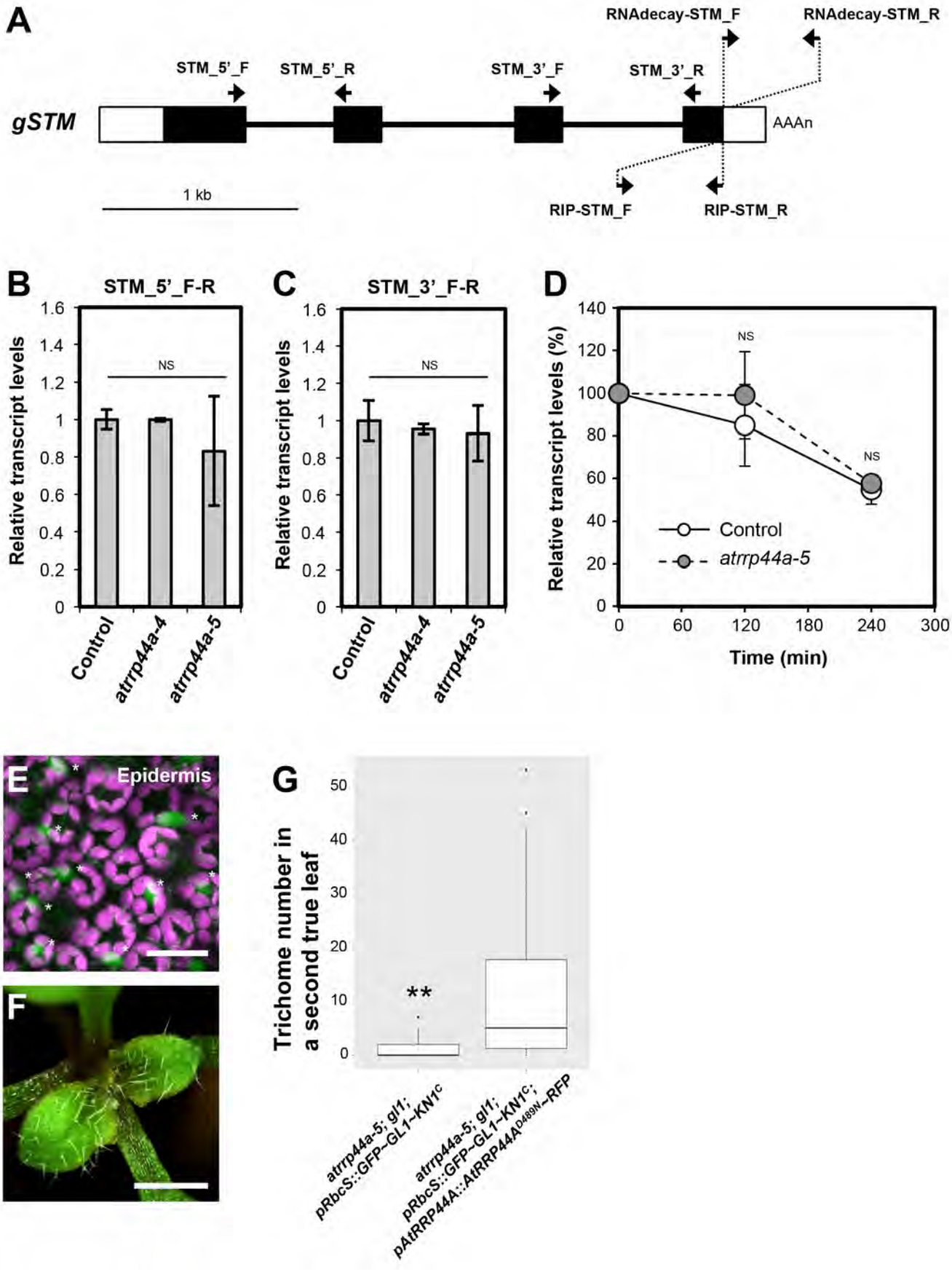
A
RNAdecay-STM_F
RNAdecay-STM_R
STM_5'_F
STM_5'_R
STM_3'_F
STM_3'_R
gSTM
AAAn
1 kb
RIP-STM_F
RIP-STM_R
B
STM_5'_F-R
Relative transcript levels
NS
Control
atrrp44a-4
atrrp44a-5
C
STM_3'_F-R
D
Relative transcript levels (%)
Time (min)
Control
atrrp44a-5
E
Epidermis
F
G
Trichome number in a second true leaf
**
atrrp44a-5; gl1; pRbcS::GFP-GL1-KN1C
atrrp44a-5; gl1; pRbcS::GFP-GL1-KN1C; pAtRRP44A::AtRRP44AD489N-RFP

349

Fig. S7. AtRRP44A is involved in KN1 trafficking independently of its catalytic function. (A) Two pairs of primers were designed at the 5' and 3' regions of *STM* for RT-qPCR (A, arrows; STM_5'_F and R, and STM_3'_F and R, respectively), and the primers for RIP-qPCR (RIP-STM_F and R) were designed near the STM stop codon. The primers for mRNA decay analysis (RNAdecay-STM_F and R) were designed on the STM 3' UTR. The sequences of all primers are listed in table S1. (B and C) RT-qPCR indicated that there was no difference in STM mRNA levels between *atrrp44a* mutants and the control lines. NS: non-significance ($P > 0.272$, Tukey HSD test). (D) mRNA decay analysis indicated that there was no difference in the rate of *STM* mRNA decay between *atrrp44a-5* mutants and the control lines. NS: non-significance ($P > 0.432$, Welch's *t*-test). Error bars in (B-D) denote SD. (E-G) A non-catalytic AtRRP44A-RFP fusion (AtRRP44A^{D489N}~RFP) recovered GFP~GL1~KN1^{c} trafficking from the mesophyll layer to the epidermis in *atrrpa44-5; gl1; pRbcS::GFP~GL1~KN1^{c}* plants (E, green, asterisks) and trichome formation was also rescued (F and G, **: $P < 0.01$ [Welch's *t*-test]). The second true leaves of plants grown for 12 days under long-day conditions were used for the trichome rescue assay. N = 49 (*atrrp44a-5; gl1; pRbcS::GFP~GL1~KN1^{c}*) and 106 (*atrrp44a-5; gl1; pRbcS::GFP~GL1~KN1^{c}; pAtRRP44A::AtRRP44A^{D489N}~RFP*). Scale bars = 20 μm (E) and 1 mm (F).

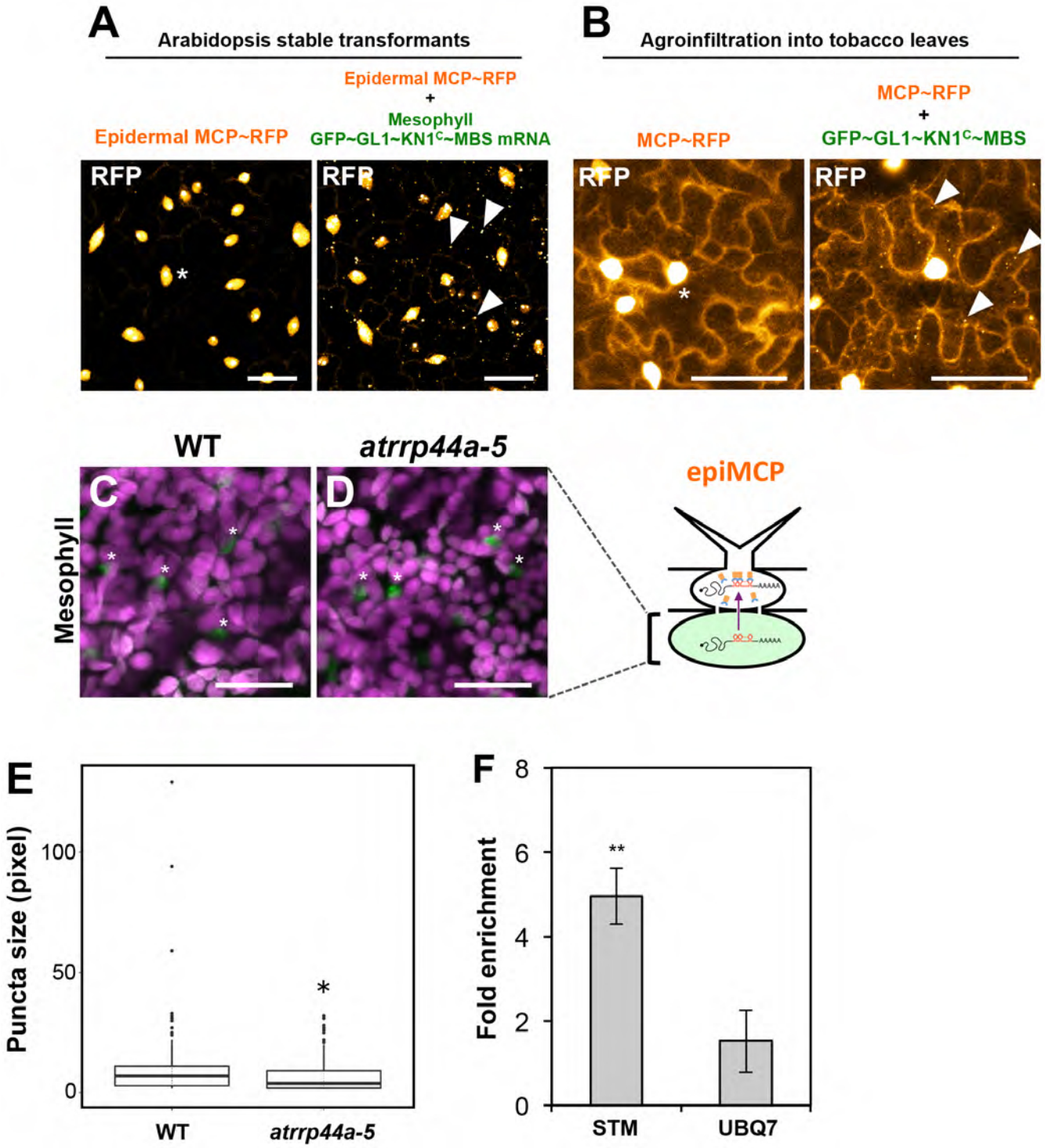

Fig. S8. Visualization of cell-to-cell trafficking of GFP~GL1~KN1^{c} mRNA *in vivo* by MS2 tagging. (A) MCP~RFP (orange) expressed alone in the Arabidopsis epidermis accumulated in nuclei

(asterisk), and the cytoplasm did not have any signal, whereas fluorescent puncta (arrowheads) were detected when GFP~GL1~KN1^{c}~MBS was expressed in the mesophyll layer, presumably reflecting trafficking of GFP~GL1~KN1^{c}~MBS to the epidermis. MCP: MS2 coat protein, MBS: MS2 bacteriophage binding sequence. Scale bars = 20 μm. (B) Cytoplasmic fluorescent puncta were not detected when *MCP~RFP* was expressed alone into tobacco leaves, whereas they were detected when co-expressed with GFP~GL1~KN1^{c}~MBS mRNA (arrowheads). Scale bars = 50 μm. (C and D) GFP~GL1~KN1^{c} protein accumulated to similar levels in the mesophyll cells of both epiMCP WT and epiMCP *atrrp44a-5* lines (asterisks). Scale bar = 20 μm. (E) Measurements of GFP~GL1~KN1^{c}~MBS mRNA puncta indicated that *atrrp44a-5* mutants had smaller puncta than WT. *: $P = 0.024$ (Welch's *t*-test). (F) RNA-immunoprecipitation (RIP) qPCR assays found association of AtRRP44A~RFP with STM transcripts *in vivo*. Enrichment of UBIQUITIN 7 (UBQ7) serves as a negative control. **: $P <$ 0.01 (Welch's *t*-test). Error bars denote SD.

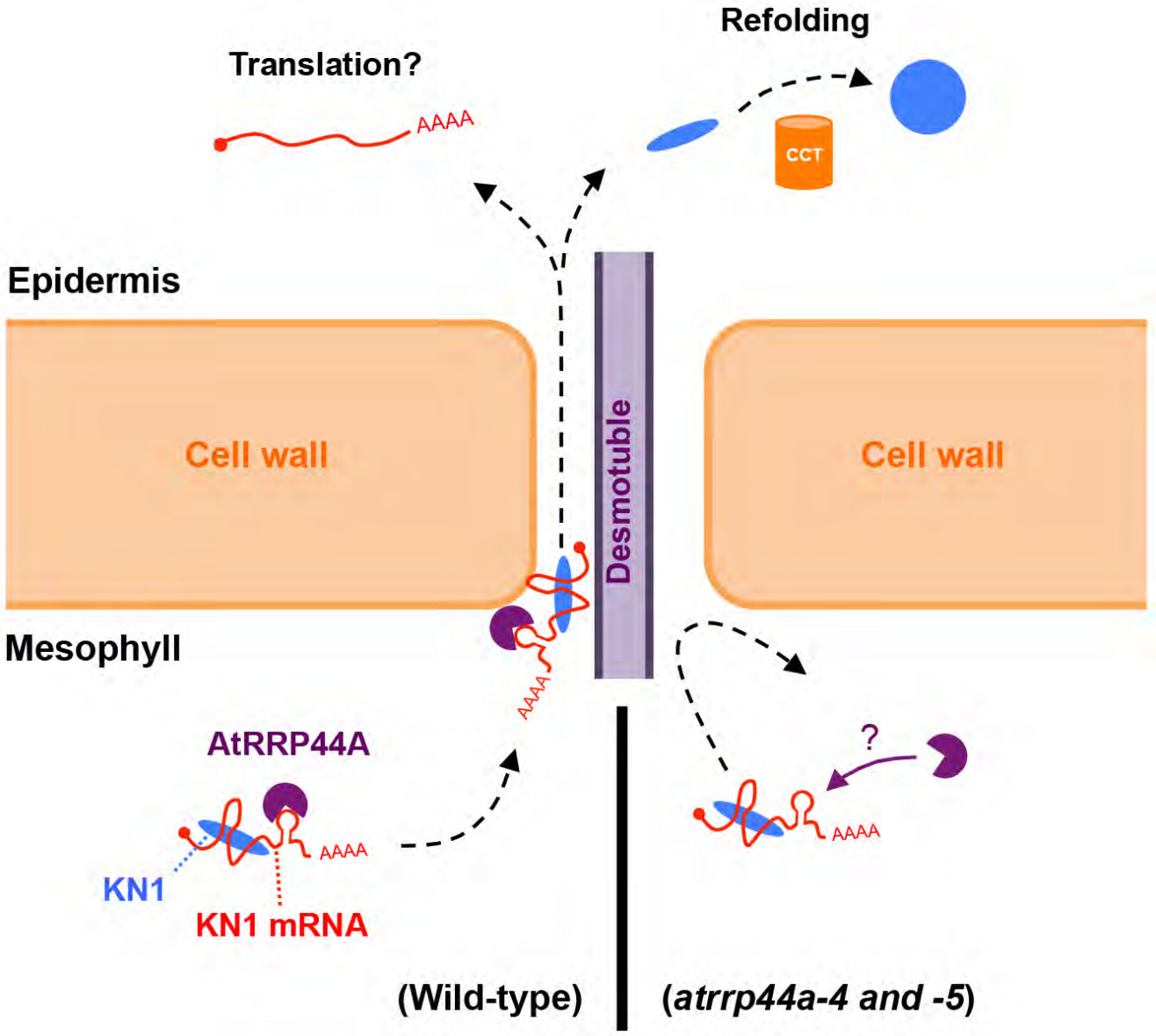

Fig. S9. A model showing the role of AtRRP44A in plasmodesmal transport of a KN1 mRNP complex. AtRRP44A binds KN1 (or STM) mRNA, possibly as an mRNP complex, and targets it to the plasmodesmata. After trafficking to the neighboring cell, the released KN1 (or STM) protein is refolded by the chaperonin (CCT) complex (*7*) and KN1 mRNA may be translated.

Table S1. Oligonucleotides used as primers in this study.

Genotyping			
Genotype	Primer name	Sequence	Note
atrrp44a-1 (SALK_037533)	atrrp44a-1_RP	AGCCATGGTTTCTGGATGAC	PCRs were performed with LBb1.3 primer (http://signal.salk.edu/tdnaprimers.2.html)
	atrrp44a-1_LP	AAATTCCAACACAAAGGGAATG	
atrrp44a-4	atrrp44a-4_F	CATTCCCTTTGTGTTGGAATTT	PCR product was digested with MwoI. WT: ~30 bp / ~60 bp, *atrrp44a-4*: 93 bp.
	atrrp44a-4_R	TGCAAGCCTTTCCACATCAGCGCTAAGAGAG	
atrrp44a-5	atrrp44a-5_F	CGCAGGCTGTGTACTTCTGT	PCR product was digested with BslI. WT: ~20 bp / ~100 bp, *atrrp44a-5*: 124 bp.
	atrrp44a-5_R	AGTTATCACTTACCGGCATATCCACGGATA	
stm-10	stm-10_F	AGGAAGAAAGGAAAGCTCCCTA	PCR product was digested with BccI. WT: 100 bp, *stm-10*: ~50 bp / ~50 bp
	stm-10_R	AAGGGAAGAGAGTTACCGAAGG	
cct8-1	cct8-1_F	TCTGTGCAGGTTATTTGCCCTTAAATATG	PCR product was digested with MwoI. WT: ~30 bp / ~80 bp, *cct8-1*: 113 bp.
	cct8-1_R	AATTGCTCCGTTCACCAAAG	

RT-qPCR, mRNA decay assay, and RIP qPCR	
Primer name	Sequence
STM_3'_F	TGGAGCCGTCACTACAAATG
STM_3'_R	GCCGTTTCCTCTGGTTTATG
STM_5'_F	CCAAGATCATGGCTCATCCT
STM_5'_R	CCTGTTGGTCCCATAGATGC
WUS_F	GGATCATCATTACTCATCTGCACCTT
WUS_R	GCCACCACATTCTTCTTCTTCTTGA
CLV3_F	GATGAAAATGGAAAGTGAATGG
CLV3_R	GGGAGCTGAAAGTTGTTTCTTG
ACT2_F	GCCATCCAAGCTGTTCTCTC
ACT2_R	ACCCTCGTAGATTGGCACAG
RNAdecay_STM_F	CATGCTTTGATCGATCCTTTAA
RNAdecay_STM_R	CCAAGTATACCGAGAACCATAGATT
RIP-STM_F	GGCTGGACCAGAAACAGATAA
RIP-STM_R	AAAGCATGGTGGAGGAGATG
RIP-UBQ7_F	TCTTCGTCAAAACCCTCACC
RIP-UBQ7_R	GGCCATCTTCCAATTGCTTA

mRNA *in situ* hybridization		
Probes	Primer name	Sequence
STM antisense	Probe_STM_F	GTTGCTTCTTCTTCTTCTCCTTCC
	Probe_STM-T7_R	GAGTAATACGACTCACTATAGGGAGAGGAATAGGAATTTCGCATAACAA
STM sense	Probe_STM-T7_F	GAGTAATACGACTCACTATAGGGAGAGTTGCTTCTTCTTCTTCTCCTTCC
	Probe_STM_R	GGAATAGGAATTTCGCATAACAA
CLV3 antisense	Probe_CLV3_F	TCTCTCTTTATCTCTCTCACTCAGTCAC
	Probe_CLV3-T7_R	GAGTAATACGACTCACTATAGGGAGACATTCACTTCAGCAACAAACG
CLV3 sense	Probe_CLV3-T7_F	GAGTAATACGACTCACTATAGGGAGATCTCTCTTTATCTCTCTCACTCAGTCAC
	Probe_CLV3_R	CATTCACTTCAGCAACAAACG
WUS antisense	Probe_WUS_F	CCAGCAAGTTGTTTTCTTGC
	Probe_WUS-T7_R	GAGTAATACGACTCACTATAGGGAGACATCATAGAGATAAAACGGTTGTCA
WUS sense	Probe_WUS-T7_F	GAGTAATACGACTCACTATAGGGAGACCAGCAAGTTGTTTTCTTGC
	Probe_WUS_R	CATCATAGAGATAAAACGGTTGTCA

* Blue characters represent the sequence of a T7 promoter.

Constructions	
Primer name	Sequence
MK1	GAAAAATCTCAGAATGGTCCGGATCAATTATGGAG
MK2	GAGCGTGTCCTCTCCCTTCAATTTCTTGCTGGAAAAC
MK3	GGAGAGGACACGCTCGAGAT
MK4	ATTCTGAGATTTTTCAAATCAGTGC
MK5	TCCGGACTCAGATCTCGAG
MK6	CAAGAGAGTGAGTTGGAGTTTCG
MK7	CAACTCACTCTCTTGGGCCGGCCTGGAGGT
MK8	AGATCTGAGTCCGGACTTGTAGAGCTCGTCCATCCC
MK9	GCTGGACTTGATATTGGCCGGCCTGGAGGTG
MK10	AATATCAAGTCCAGCCAACTTAAGAGCAAGCAAGAGAGTGAGTTGGAGTTTCG
MK11	AATGCTGCTGCTGCCACTGAAGAGGGAATATCTG
MK12	GGCAGCAGCAGCATTTTCCCTATCATTAGTTACAAGCAAC
MK13	TCGGCTGCTGCTCTTATATACCAAGAGCATAAGCCCATG
MK14	AAGAGCAGCAGCCGAAGGTCTAGAATCATCTGCATC
MK15	AGGGTTCATCAGATCTCCACCGGTATCTCGCTTC
MK16	GGCGAATTCGCGGCCGCCTAGCCGAGCCGGTACAG
MK17	CTCGAGATGGAAGGTTCAGGGAATAGAAGACATAAGCGTATGATCAAGAACAGAGAATCTGCAGCTCGTTC CCGCGCTAGGAAACAGGCTTATACAAACGGCTACCCCTACGACGTG
MK18	GGTGGCGACCGGTGG
MK19	CGGATCCACCGGTCGCCACCGTCTCTAAGGGGGAGGAGCTC
MK20	CTCGAGTTACTTGTAGAGCTCGTCCATCCC
MK21	GCTGCTGCAGATCTTGTCGACGGGAGCCTCAAGCAAGAGTT
MK22	AAAGGATCGATCAAAGCATGGTGGAGGAGATG
MK23	CACCATGCTTTGATCGATCCTTTAAAACGTTTATTTCA
MK24	GCTTGCATGCTGCAGGTCGACTGAATCAATGCTTGGTTTGG
MK25	GGATATTAATGATGCATTGCAC
MK26	TGCAATGCATCATTAATATCC

Table S2. Excitation and detection wavelengths used for confocal image acquisition for each fluorophore used in this study.

Fluorophore	Excitation wavelength (nm)	Detection wavelength (nm)
GFP	488	410-511
Chlorophyll A	640	656-700
TagRFPT	561	580-617
DAPI	405	410-469
Aniline blue (Fig. 3D)	405	410-546
Aniline blue (Fig. 4J)	405	410-470

Movie S1 and S2. Association of KN1 mRNA with plasmodesmata between Arabidopsis epidermal cells. In the *pRbcS::GFP~GL1~KN1^{c}~MBS; pML1::MCP~RFP* line, a GFP~GL1~KN1^{c}~MBS mRNA punctum (orange) was recruited to plasmodesmata at the interface between epidermal cells. Plasmodesmata were stained by aniline blue (blue).

Movie S3. Association of KN1 mRNA with plasmodesmata between Arabidopsis epidermal and mesophyll cells. In the *pRbcS::GFP~GL1~KN1^{c}~MBS; pRbcS::MCP~RFP* line, a GFP~GL1~KN1^{c}~MBS mRNA punctum (orange) was recruited to plasmodesmata at the interface between an epidermal and a mesophyll cell. Plasmodesmata were stained by aniline blue (blue).

Movie S4. Association of KN1 mRNA with plasmodesmata between tobacco epidermal cells. An MBS~GFP~GL1~KN1^{c} mRNA punctum (orange) was recruited to plasmodesmata (green) at the interface between epidermal cells in a tobacco leaf. *pRbcS::MBS~GFP~GL1~KN1^{c}*, *pML1::MCP~RFP* and *p35S::PDLP1~GFP* were transiently co-expressed in tobacco leaves by agroinfiltration.

References

42. S. J. Clough, A. F. Bent, Floral dip: a simplified method for Agrobacterium-mediated transformation of Arabidopsis thaliana. *The plant journal* **16**, 735-743 (1998).

43. A. M. Davis, A. Hall, A. J. Millar, C. Darrah, S. J. Davis, Protocol: Streamlined sub-protocols for floral-dip transformation and selection of transformants in Arabidopsis thaliana. *Plant Methods* **5**, 3 (2009).

44. F. Xu, C. Copeland, X. Li, Protein immunoprecipitation using *Nicotiana benthamiana* transient expression system. *Bio Protoc* **5**, e1520 (2015).

45. J. Chen, S. Dellaporta, "Urea-based plant DNA miniprep"in *The maize handbook*. (Springer, New York, 1994), pp. 526-527.

46. R. Zavaliev, B. L. Epel, "Imaging callose at plasmodesmata using aniline blue: quantitative confocal microscopy"in *Plasmodesmata*. (Springer, New York, 2015), pp. 105-119.

47. D. Jackson, B. Veit, S. Hake, Expression of maize *KNOTTED1* related homeobox genes in the shoot apical meristem predicts patterns of morphogenesis in the vegetative shoot. *Development* **120**, 405-413 (1994).

48. G. Wu, E. P. Spalding, Separate functions for nuclear and cytoplasmic cryptochrome 1 during photomorphogenesis of Arabidopsis seedlings. *Proceedings of the National Academy of Sciences* **104**, 18813-18818 (2007).